D. Kreeft

Effect of the Tip Shape on the Steerability of a Bioinspired Needle

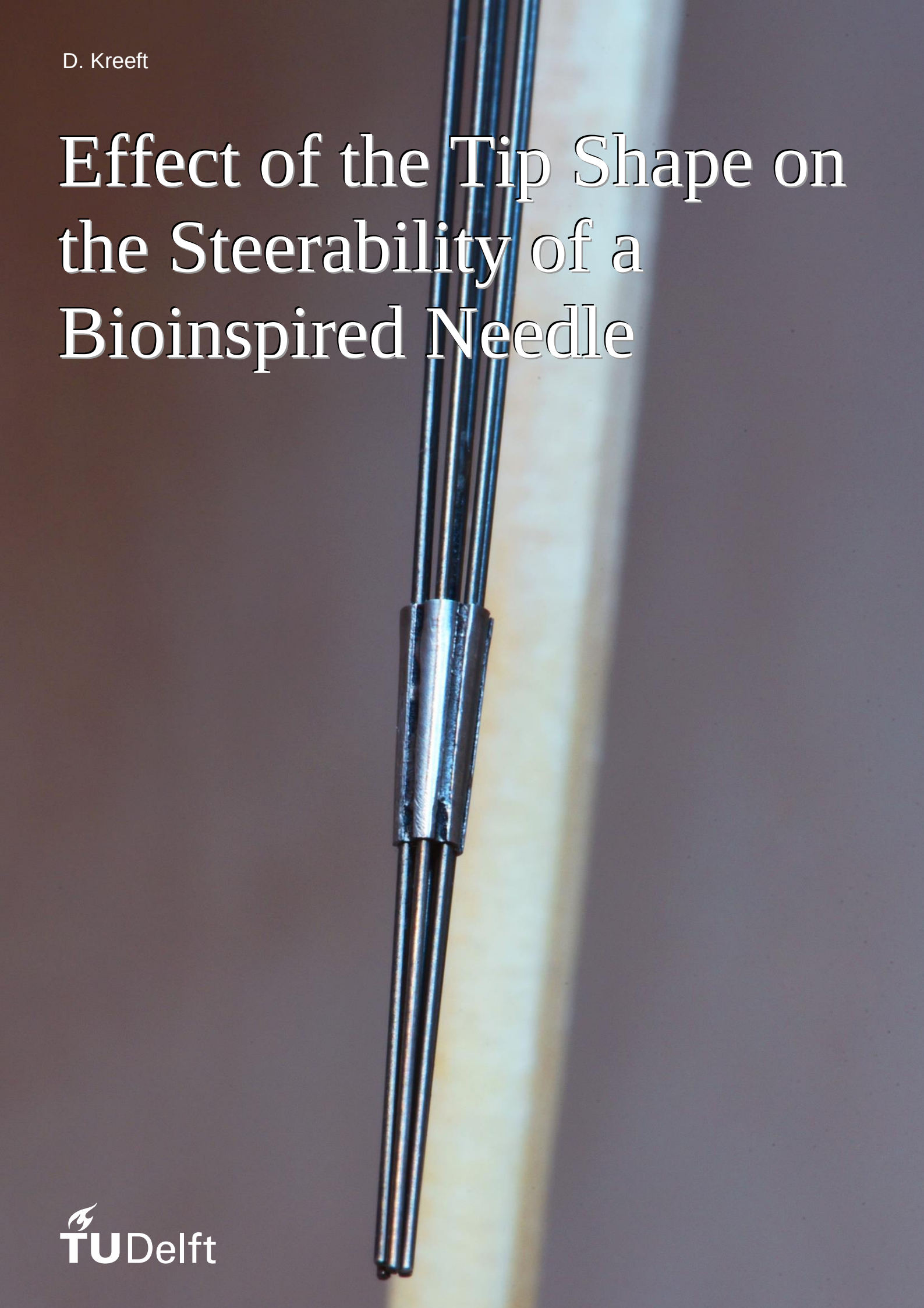

TU Delft

Effect of the Tip Shape on the Steerability of a Bioinspired Needle

By

D. Kreeft

in partial fulfilment of the requirements for the degree of

Master of Science
in Mechanical Engineering

at the Delft University of Technology,
to be defended publicly on Thursday December 22, 2016 at 02:00 PM.

Supervisors:	Ir. M. Scali	
	Dr. D. Dodou	
	Prof. dr. ir. P. Breedveld	
Thesis committee:	Prof. dr. ir. P. Breedveld,	TU Delft
	Dr. D. Dodou,	TU Delft
	Dr. ir. M. Langelaar,	TU Delft
	Ir. M. Scali,	TU Delft

TU Delft

Effect of the Tip Shape on the Steerability of a Bioinspired Needle

D. Kreeft

***Abstract*—Many types of percutaneous procedures require a high accuracy and precision in needle targeting. The use of steerable needles is promising to meet these requirements. At TU Delft, a novel steerable needle prototype inspired by the ovipositor of a parasitoid wasp has been developed. The prototype consists of six actuated outer wires, encircling a seventh central wire, that move in linear reciprocally. The outer wires are held together by an interlocking mechanism that is attached to the central wire at the tip of the needle. Despite the interlocking mechanism, a problem of the prototype is that the wires tend to bifurcate and therefore each wire is apt to move forward in an undesired direction when advanced within a substrate, affecting the steerability (i.e., the maximum curvature that the needle is able to produce when steering). To control the amount of bifurcation and to increase the steerability of the prototype, two new interlocking mechanism designs were tested: one making the wires converge and another making the wires diverge. The prototype with each of the interlocking mechanism designs was tested in terms of 1) the energy conversion efficiency and 2) the resulted curvatures when advancing through a gelatin substrate. The problem of bifurcation was solved. Results showed the highest energy conversion efficiency (i.e., 70%) for the interlocking mechanism that converged wires, and the highest average curvature (i.e., 0.0226 cm^{-1}) for the interlocking mechanism that diverged wires. Conclusively, when an efficient insertion is not necessary, the needle with an interlocking mechanism that diverges the wires is the most desired to explore further as it exhibits the highest steerability.**

***Index Terms*—Percutaneous surgery, steerable needle, biologically inspired design, ovipositor-inspired needle.**

I. Introduction

TRADITIONAL rigid needles often follow straight paths, thereby limiting the surgeon during percutaneous procedures, e.g., when trying to avoid penetrating organs [1]. Flexible needles might allow for curved paths, but could suffer from undesired deviations from the desired needle path due to tissue properties (e.g., inhomogeneity and anisotropy) or physiological processes (e.g., fluid flow and respiration) [2]. In addition, some procedures such as biopsies, radiotherapy, and localized drug delivery require a high precision and accuracy in targeting, as needle placement errors and tissue movement increases the risk of false diagnoses [3, 4] (including understaging [5]), poor dosimetry [6-9], or even tissue morbidity [10]. Other unplanned and undesired effects could also be harmful to the patient: The withdrawal and reinsertion of the needle in case of misplacement could lead to an elongated procedure and damage to organs or the puncture of vessels [11]. A possible way to circumvent undesired deviations from the intended needle path and to avoid associated risks is to use steerable needle instruments that allow for passive or active steering.

Mr. D. Kreeft is with the Department of Biomechanical Engineering, Delft University of Technology, Mekelweg 2, 2628 CD Delft, Netherlands (e-mail: d.kreeft@outlook.com).

A. State-of-the-art on steerable needles

Several examples of steerable needle instruments can be found in literature (see [12] for an example), including those that make use of path planning systems and robotics [13]. A simple form of a steerable needle instrument is a flexible needle with a bevel-tip that bends when inserted into soft tissues due to an asymmetric load on the tip [2, 14, 15]. Several variations on bevel-tip needles include lancet needles [16] and kinked bevel-tip needles that allow for an additional degree of freedom to aid bending [17]. Furthermore, pre-bent or pre-curved needles allow for bending in one [18] or two planes [19, 20]. For example, bending in two planes can be achieved by using pre-curved concentric tubes that are able to move independently [21]. Other types of steerable needles make use of actuated elements, often driven by cables [22-24].

As a main drawback, flexible steerable needle instruments are prone to buckling near the entry point or within tissue, especially when advanced deep inside the tissue [17, 25, 26]. In addition, most existing bevel-tip flexible needles are limited in maneuverability to only one plane (2D steering). By axial rotation of the whole body (i.e., "duty cycling" [27]), the amount of steering could be changed. However, duty cycling could cause the needle to twist, thereby introducing torsion in the needle between its base and the tip. The resulting twist angle increases the difficulty to control the needle trajectory [28, 29].

Some steerable needle designs are inspired by the ovipositor of a parasitoid wasp. The shape of this egg-laying organ resembles a needle and its elements allow for penetration into and 3D steering inside substrates by moving back and forth reciprocally. This insertion process, whereby one of the elements is pushed further into the substrate, while another is being pulled back, has been shown to reduce the risk of buckling [30]. The mechanics of the ovipositor thus provide a good starting point for the design of slender steerable needle instruments [31-34].

Currently, two steerable needle prototypes inspired by the parasitoid wasp ovipositor are described in literature. First,

Frasson et al. [31] created a needle prototype of which the base of the needle consists of two or four slender parts that are interlocked together by a jigsaw puzzle-like mechanism [35, 36]. The parts can move independently and can thereby be offset relative to each other [37]. The offset determines the steering direction when inserting the needle into a substrate. Second, Scali et al. [38] developed a needle prototype consisting of six individually controlled nitinol wires positioned in a circle and one stationary central nitinol wire [39]. The six wires are moved back and forth reciprocally and are held together by an interlocking mechanism that is glued to the stationary central wire, an alignment ring that is fixed to a reference point to ensure a correct radial orientation, and five support rings (see Figure 1 for a schematic overview). By actuating one or two wires simultaneously, the needle can advance within a substrate as the remaining stationary wires provide the required friction force to compensate for the forward motion of the actuated wire(s). In addition, by offsetting the wires, an asymmetric tip similar to a bevel-tip needle can be created.

B. State-of-the-art on radii of curvatures

The steerability of needle instruments is often expressed by the minimum achievable radius of curvature, i.e., the radius of the circular arc which best approximates the curve at the point of maximum steering. As described by Misra et al. [40, 41], the radius of curvature of a bevel-tip needle is probably a function of 1) the substrate elasticity or the elastic modulus of the needle, 2) the second moment of inertia, 3) the tip bevel angle, and 4) the friction coefficient. The radius of curvature is also inversely proportional to 1) the substrate elasticity or the elastic modulus of the needle, and 2) the substrate rupture toughness. Majewicz et al. [42] found that their bevel-tip nitinol needle curved more in kidney than in liver and prostate, which could be due to organ size, tissue inhomogeneity, and stiffness (kidney is possibly less stiff than liver [43] or prostate [44]); thus partly corresponding to the findings by Misra et al. [40, 41]. The results of a literature review on the smallest achieved radii of curvature are summarized in Table I.

The ovipositor-inspired needle developed by Scali et al. [38] generated on average curvatures up to 0.0184 cm^{-1}, i.e., a radius of 54.35 cm, depending on the mode of actuation [39]. However, the wires which the needle consisted of were not completely straight, limiting the conclusiveness of the results [39]. In addition, the wires tended to disperse (i.e., spread out), and therefore each wire was apt to continue in an undesired direction when advanced within the gelatin substrate. This phenomenon, henceforth referred to as ‘bifurcation’, possibly resulted in the radius of curvature of the ovipositor-inspired needle being higher than previous ovipositor-inspired steerable needle designs [27, 34]. Further improvements in the ovipositor-inspired needle are thus required to minimize the bias and bifurcation of the wires.

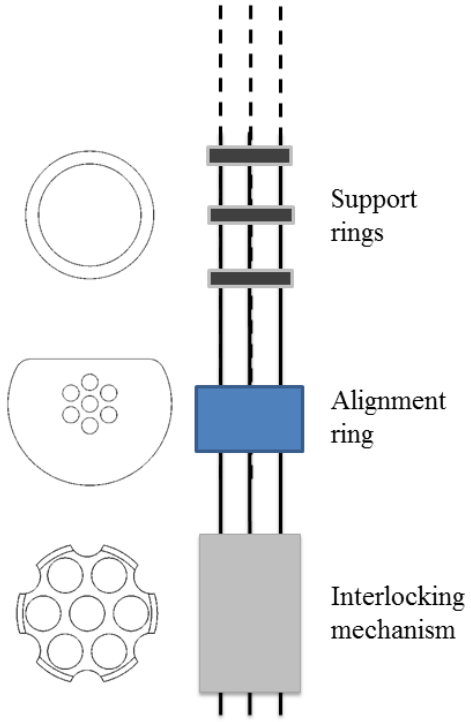

Figure 1: Schematic overview of the support (in black) and alignment ring(s) (in blue), and the interlocking mechanism (in grey) of the ovipositor-inspired needle. The tip is pointing downwards. On the left, the frontal view of the aforementioned parts is shown.

C. Goal of thesis

This thesis describes an ovipositor-inspired needle with different tip designs and the subsequent experimental validation of the needle prototype with each tip design. The altered tip designs possibly allow for more control over the amount of bifurcation. By conducting two types of experiments to test each of the tip designs, the amount of bifurcation and the steerability of the needle prototype with the different tips is determined. The research aims to contribute towards the ultimate goal of decreasing the radius of curvature of the ovipositor-inspired needle.

First, the design objective and conceptual design is described. Next, the final design is presented, and the actuation methods for moving straight and steering are described. The experimental setup, design, and procedure are explained, and the experimental results are presented. Finally the results are discussed, and recommendations for future work are provided.

II. Design

A. Design objective

In order to prevent the wires from bifurcating, the objective is to design a solution for the previous ovipositor-inspired needle [39] and to minimize the radius of curvature, i.e., to increase steerability. In order to be compatible with existing surgical equipment for, e.g., biopsy [45], it is of importance to not exceed the diameter of 14-gauge (approximately 2.1 mm).

TABLE I: SUMMARY OF RADII OF CURVATURE FOUND IN LITERATURE

Ref.	Category	Outer diameter [mm]	Smallest bending radius [cm]	Insertion depth [cm]	Insertion speed [mm/s]	Substrate	Medical application
[42]	Nitinol pre-bent (15°) bevel tip (30°) needle	0.58	5.62 (ex vivo), 10.5 (in vivo)	5 (in vivo, ex vivo not specified)	5	Kidney (canine)	
[49]	Nitinol pre-bent (45°) bevel tip needle	0.58	3.4 (ex vivo)	10	15	Liver (goat)	Ablation, biopsy, brachytherapy
[50]	Flexure-tip (max. 22°) needle (joint at 4 mm from tip) with 10° bevel	0.91	12.1 (gelatin), 17.6 (ex vivo)		5	10% gelatin, Pork loin	
[51]	Custom built pre-bent (6.3 mm from tip) nitinol wire with stainless steel bevel (10°) needle tip	1.27 stainless steel tip, 0.28 nitinol wire	5.2	10		6.5% gelatin	
[52]	Nitinol bevel tip (7°) wire	0.52	33.3	6		medical training model (#60502 Percutaneous Nephrolithotomy Slab, Limbs & Things, Inc., Savannah, Ga.),	Access to the kidney
[53]				23.5			
[2, 8]	Nitinol wires with bevel tip (38.0°)	0.40	16.1–17.94 (varies throughout insertion)	20	2.5	Plastisol tissue	
[19]	Curved set of concentric tubes	1.684	10.62	7.58			
[27]	Four-segment needle (STING)	4	9.73		0.5		
[48]	Pre-bent (~16° at 6.3 mm from tip) nitinol wire with bevel tip (~20°)	~0.15		11			Burr hole craniostomy
[23]	Seeker Steerable Biopsy Needle™ [54]		23.8				Lung biopsy
[20]	Concentric tubes (inner tube: d_{in} = 0.97 mm, d_{out} = 1.14 mm)	1.38	17.8			10 wt% gelatin	Transoral access to the lung
[34]	Four-segment needle (STING)	8	5.88		1	6 wt% gelatin	

B. Conceptual design

Decreasing radius of curvature

The resulting curvature of steerable needles could be increased by: 1) decreasing the needle diameter [42, 46] as this lowers the area moment of inertia, resulting in lower resistance to needle bending [47]; 2) increasing the surface area at the bevel edge [48] to increase the influence of the resulting lateral forces; 3) decreasing the bevel angle [26] as this increases the asymmetry of the tip and thereby the lateral force acting on the tip; 4) using a pre-bent needle tip [49, 55-57]; 5) introducing an additional hinge at the tip [50, 58] thatincreases the deflection angle [12], and 6) changing the needle material [59] to lower its bending stiffness [60].

The diameter of the ovipositor-inspired needle depends on the diameter of the interlocking mechanism that is directly affected by the diameter of a single wire and the number of wires used. Decreasing the wire diameter will lead to lower resistance to bending as the protruding element diameter consisting of 1 or 2 wires is decreased. However, the degree of buckling is likely to be increased; the equation to calculate the critical load for a column is given by

$$P = \frac{\pi^2 EI}{(KL)^2} \quad (1)$$

where P is the critical load of the column: the maximum load a column can bear while staying straight, E the elastic modulus of the column (in the case of the ovipositor-inspired needle the wire), I the area moment of inertia of the column, L the unsupported length of the column, and K the column effective length factor. For example, when decreasing the diameter of a wire from 0.25 to 0.18 mm, the critical load is already less than 1/6 of the original critical load. This leads to a need for more buckling support, which could either add to the needle diameter or decrease the needle length. Increasing the needle diameter also increases the surface area at the bevel edge. However, increasing the diameter leads to a greater resistance to bending, a scaling effect which is more influential than the gain in surface area at the bevel edge [47].

The effect of the bevel angle on the resulting curvature decreases by reducing the needle diameter [32], as decreasing the needle diameter reduces the lateral force on the tip [61]. The same was also hypothesized by Frasson et al. [32]. On the contrary, the effect of the bevel angle might not be present due to tissue inhomogeneity that increases the variance of the resulting curvatures [49]. In addition, O'Leary et al. [62] could not establish significant correlations between the axial forces and the bevel angle either [63].

In order to steer with a pre-bent needle or kinked tip, duty

cycling could be used [50, 51]. However, introducing a pre-bent needle tip could cause damage to the tissue surrounding the tip when the needle is twisted [25, 64, 65], placing constraints on planning and control algorithms [56, 66].

The bending stiffness is a function of elastic modulus and area moment of inertia. By changing the needle material, the different elastic modulus could alter the bending stiffness. Nonetheless, the nitinol that is used for the wires of ovipositor-inspired needle has an elastic modulus of 28–40 GPa, depending on its structure, which is already lower than that of stainless steel alloys [67] often used for needles.

In summary, the curvature of a bevel-tip needle could be increased by lowering the area moment of inertia (e.g., by changing the geometry) or by lowering the elastic modulus (e.g., by changing the material). In addition, the shape of the tip could be changed, although the effects of this alteration are not decisively established.

Controlling bifurcation

First, as a possible origin for the bifurcation, the tolerances between the wires and the interlocking mechanism are considered. The space between a wire and the interlocking mechanism could cause the wires to exhibit play. The play could lead to the wires bending within the interlocking mechanism, assisting the bifurcation. Possible solutions include lowering these tolerances by increasing the diameter of the wires or by decreasing the size of the holes of the interlocking mechanism.

Another solution is to increase the length of the interlocking mechanism. Deflection of the wires can be approximated by

$$\kappa(x) = \frac{M(x)}{E(x)I(x)} \quad (2)$$

where κ is the curvature, M the internal bending moment, E the elastic modulus, and I the area moment of inertia. Increasing the length of the interlocking mechanism effectively decreases the internal bending moment as the moment arm is decreased. Elongating the interlocking mechanism thus prevents the wires from bending as the local bending resistance is larger.

As a first tip design change to control the bifurcation, an elongated (from 2 to 5 mm as compared to the previous iteration of the ovipositor-inspired needle [39]) cylindrical interlocking mechanism is considered. The 5-mm cylindrical interlocking mechanism would have holes with a small tolerance, ensuring that the wires therein are not able to bend inside the part due to a gap between the two. As a second tip design change, a conical interlocking mechanism design is considered. Such an interlocking mechanism design introduces a tendency for the wires to move towards or away from the central wire and thus a possible way to control the bifurcation. By changing the angle of attack of the wires of the ovipositor-inspired needle (i.e., the angle of the wires with respect to the longitudinal axis of needle), the wires could mimic a pre-curved needle.

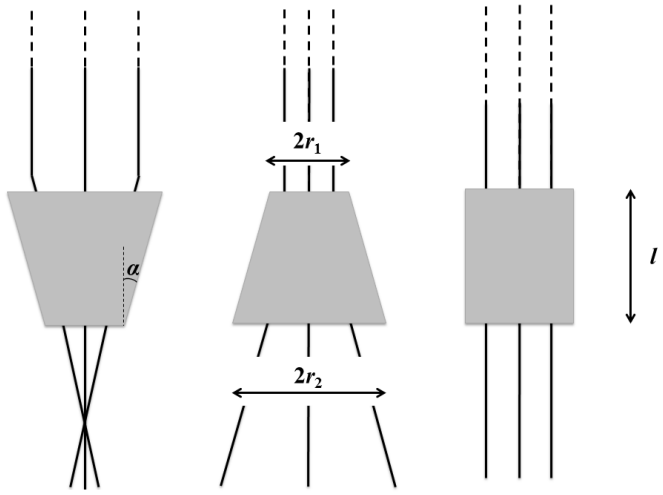

Figure 2: The three interlocking mechanism designs displayed from the top (in gray). The black lines indicate the wires and the dashed lines indicate that the wires continue toward the needle base. The tip is pointing downwards. From left to right: conical (i.e., converging and diverging) and cylindrical interlocking mechanism designs. Displayed are the design parameters angle α, radii r_1, r_2, and length l.

The conical interlocking mechanism has several design parameters, including its length l and its angle α as is shown in Figure 2. There is a tradeoff between both design parameters as increasing the length of the mechanism under the same angle would lead to a larger diameter. Similarly, increasing the angle under the same length would lead to larger diameter. The relationship between the diameter, length, and half-angle of the cone is given in equation 3.

$$d_{max} = 2r_2 = 2(r_1 + l\tan\alpha) \quad (3)$$

where r_1 is the smallest and r_2 the largest diameter, l the length of the interlocking mechanism, and α the half-angle of the cone. As stated before, a larger length of the interlocking mechanism prevents the wires from bending, as the local bending resistance is larger. A larger half-angle leads to more strain on the wires at their entry point into the holes of the interlocking mechanism. In this respect, we opted for a conical interlocking mechanism design with a length of 5 mm. Subsequently an angle of 2° was chosen in order to come to a maximum diameter of approximately 1.6 mm.

C. Final prototype design

Needle tip

The ovipositor-inspired needle consists of seven straight annealed nitinol wires (⌀0.25 mm) with an activation temperature of 20 °C (the previous prototype [39] used nitinol wires with an activation temperature of 35 °C). The relatively low activation temperature ensures that the bias in the wires is minimized at room temperature. The free length of the needle depends on the total length of the wires. There is a tradeoff between the free wire length and the weight of the wires of the needle as a longer wire length requires more support rings, thereby causing the needle to deflect under its own weight. An equation for the wire length is given by

$$l_{tot} = l_{tm} + \frac{l_r(l_c - l_{crit}) + l_m l_{crit}}{l_{crit} - l_r} + l_c + l_m \quad (4)$$

where l_{tot} is the total length of a wire, l_{tm} the length of the transmission, l_r the length of one buckling support ring, l_c the desired insertion depth, l_{crit} the maximum unsupported length, and l_m represents the desired safety margin to deal with the wire possibly being able to get stuck. To prevent the needle from deflecting under its own weight, a total length of the wires equal to 250 mm was chosen.

The three interlocking mechanism designs applied in the ovipositor-inspired needle are made out of stainless steel and are shown in Figure 2. The three designs consist of six holes (⌀0.3 mm) positioned along the outer rims of the part and one central hole (⌀0.3 mm). The central wire is placed into the central hole of the interlocking mechanism, and glued to it. The six remaining wires are positioned inside the holes on the rim of the interlocking mechanism and are free to slide back and forth.

The first interlocking mechanism design has a conical shape with its apex at the distal end of the needle and is henceforth referred to as converging interlocking mechanism, see Figure 3a. The second design consists of a conical shape with its base at the distal end and is further referred to as diverging interlocking mechanism. The converging interlocking mechanism makes the wires converge by having an increased diameter ($d = 1.55$ mm) on the proximal side of the needle with respect to the needle base. The diverging interlocking mechanism makes the wires diverge as it is the opposite of the converging interlocking mechanism. Thus, this design has the same dimensions as the converging design and therefore has an increased diameter on the distal side of the needle. The angle of the wires with respect to the centerline of the ring in both designs is 2°. The engineering drawings of the conical interlocking mechanism and the third design having a cylindrical shape ($d = 1.2$ mm) are shown in Appendix A, together with more information about the fabrication process of the interlocking mechanisms.

Two alignment rings made from aluminum are positioned before the interlocking mechanism to support the needle and to provide a consistent insertion position with respect to the gelatin. They consist of seven holes (⌀0.3 mm) and are shaped semi-cylindrically ($d = 3.0$ mm, l = 2 mm) to be fastened to a reference point such as the needle base. The wires are free to slide through the alignment rings that are positioned between the interlocking mechanism and the support rings. The six support rings ($d = 1.0$ mm, l = 2 mm) are made out of stainless steel and are positioned evenly along the length of the needle.

Needle base

Six stepper motors (Faulhaber AM0820) actuate the six outer wires of the ovipositor-inspired needle. In this way, each wire can be controlled independently. The motors are housed in an aluminum actuation unit that also houses the transmission, see Figure 3b. Each of the wires has a

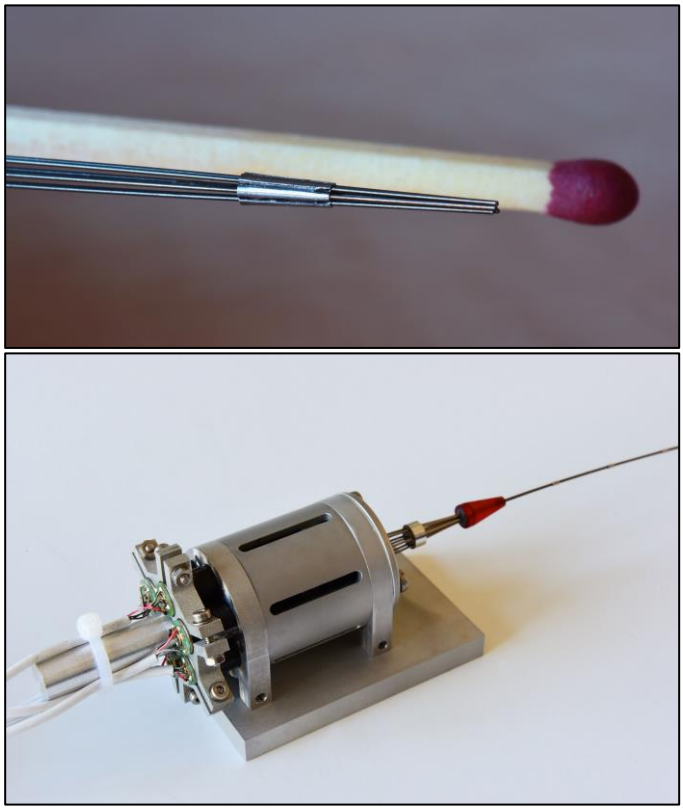

Figure 3: a) (top) photograph of the converging interlocking mechanism and the wires of the needle. A matchstick is shown for reference; b) (bottom) photograph of the housing of the needle. Shown are the stepper motors, the transmission, and the funnel that bundles the wires of the needle coming out of the housing.

transmission that consists of a leadscrew and a slider to convert rotational motion of the stepper motors into a linear reciprocal motion of the wires. The cylindrical housing (l = 85 mm, d = 40 mm) has ducts to ensure the sliders move along one axis. Besides, the housing can be attached to a foundation by using four supports to fix the position of the ovipositor-inspired needle. Seven stainless steel tubes are attached to the housing to guide the seven wires to form a bundle. In addition, a rapid prototyped funnel at the end of the tubes ensures that the wires cannot change their position relative to each other.

D. Actuation of the needle

Forward motion

The forward motion of the needle is as follows. Either one or two wires are actuated forward simultaneously. These modes of actuation are referred to as single wire and double wire actuation, respectively. After all wires have been moved forward over a predefined distance, called the stroke, all six wires are retracted over the same distance simultaneously, causing the interlocking mechanism with the central wire to advance within the substrate. This sequence is henceforward referred to as a cycle. The theoretical traveling distance is the distance the needle would travel into the substrate in case of no losses and can be calculated as the total number of cycles times the stroke. Losses during the motion of the wires of the needle could be due to slip between the wires and substrate

when advancing the wires into the substrate.

During the forward motion of the prototype, assuming the forces of the protruding wire(s) are fully compensated for by the stationary wires and thus no slip occurs, the force equation can be expressed as

$$m\left(F_{c,w} + F_{d,w}\right) \leq mF_{a,w} \leq nF_{s,w} + F_{s,i} \quad (5)$$

where m is the number of wires that move forward at a given time, $F_{c,w}$ the cutting force of a wire, $F_{d,w}$ the dynamic friction force of a moving wire with the substrate, $F_{a,w}$ the axial insertion force of a wire delivered by the stepper motor, n the number of stationary wires, $F_{s,w}$ the static friction force between a stationary wire and the substrate, and $F_{s,i}$ the static friction force between the interlocking mechanism and the substrate. In case the friction and cutting forces are not fully compensated for, slip between the needle and the substrate occurs, and thus the force balance is not met. The free body diagram of the interlocking mechanism during the forward motion of the cycle is shown in Figure 4.

During the backward motion of the prototype, when the interlocking mechanism is advanced within the substrate by retracting all six outer wires, the force equation can be expressed as

$$F_{c,i} + F_{d,i} \leq (m+n)F_{a,w} \leq (m+n)F_{s,w} \quad (6)$$

where $F_{c,i}$ is the cutting force of the interlocking mechanism and $F_{d,i}$ is the dynamic friction force of the interlocking mechanism with the substrate. The free body diagram of the interlocking mechanism during the backward motion of the cycle is shown in Figure 4.

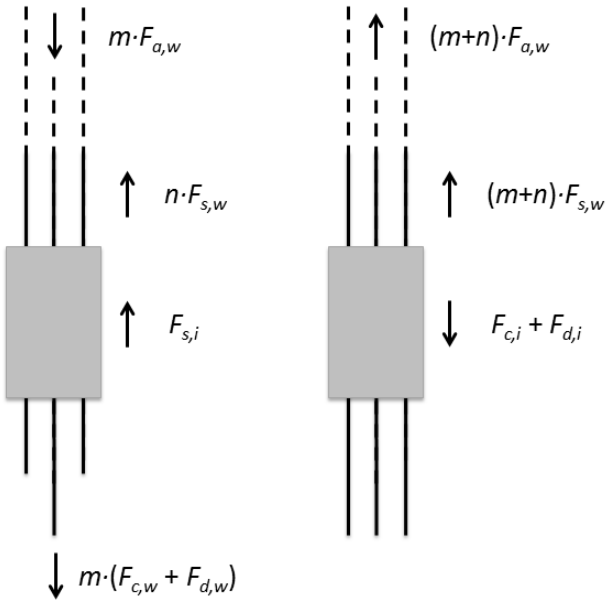

Figure 4: (left) the free body diagram of the interlocking mechanism during the forward motion of the actuation cycle. m is the number of wires that move forward at a given time, $F_{c,w}$ the cutting force of a wire, $F_{d,w}$ the dynamic friction force of a moving wire with the substrate, $F_{a,w}$ the axial insertion force of a wire delivered by the stepper motor, n the number of stationary wires, $F_{s,w}$ the static friction force between a stationary wire and the substrate, and $F_{s,i}$ the static friction force between the interlocking mechanism and the substrate; (right) the free body diagram of the interlocking mechanism during the backward motion of the actuation cycle. $F_{c,i}$ the cutting force of the interlocking mechanism and $F_{d,i}$ is the dynamic friction force of the interlocking mechanism with the substrate. The tip is pointing downwards; the dashed lines indicate that the wires continue until the needle base.

Steering

The cycle of the needle steering with a cylindrical interlocking mechanism is as depicted in Figure 5. Initially, a bevel offset is created by moving a pair of wires forward over a predefined distance, recreating a needle tip that resembles a bevel-tip (although 'discrete'). The pair of wires that is moved forward depends on the desired steering direction: wires 5 and 6 for steering to the left and wires 2 and 3 for steering to the right. After the initialization, the first pair (i.e., wires 1 and 6 for steering to the left; wires 1 and 2 for steering to the right) is advanced over a predefined distance (i.e., the 'stroke'). The asymmetric tip forces that arise due to one of the wires being offset causes the pair of wires to deflect. The next pair (i.e., wires 4 and 5 for steering to the left; wires 3 and 4 for steering to the right) also deflects when moved forward an amount equal to the stroke as one of the wires of the pair is offset. The third and final pair (i.e., wires 2 and 3 for steering to the left; wires 5 and 6 for steering to the right), which does not contain an offset wire, is moved forward and follows the path cut by the previous four wires. Following the movement of the wire pairs, all six wires are retracted over the same distance simultaneously, causing the interlocking mechanism with the central wire to advance within the substrate. In summary, the steering of the ovipositor-inspired needle with a cylindrical interlocking mechanism depends on the tissue interaction forces that result from an asymmetric tip load: two out of the three pairs of outer wires contains one wire that is offset with respect to its complement wire. The asymmetric tip resembles a discrete bevel-tip needle.

The cycle of the needle steering with either of the two conical interlocking mechanisms is depicted in Figure 5. Initially, an offset is created by moving four of the wires of the needle forward over a predefined distance (i.e., the 'offset'). For steering to the left, the following wires are offset: 1, 2, 3, and 4 for the converging and wires 1, 4, 5, and 6 for the diverging interlocking mechanism. For steering towards to right, the aforementioned set of four wires is interchanged between the two conical interlocking mechanisms. The wires that are offset will always maintain at least the offset distance relative to the wires that are not offset (i.e., wires 2 and 3 when the left side protrudes; wires 5 and 6 when the right side protrudes) as the offset wires are the first to be actuated after being offset. The first pair of wires is actuated forward (i.e.,

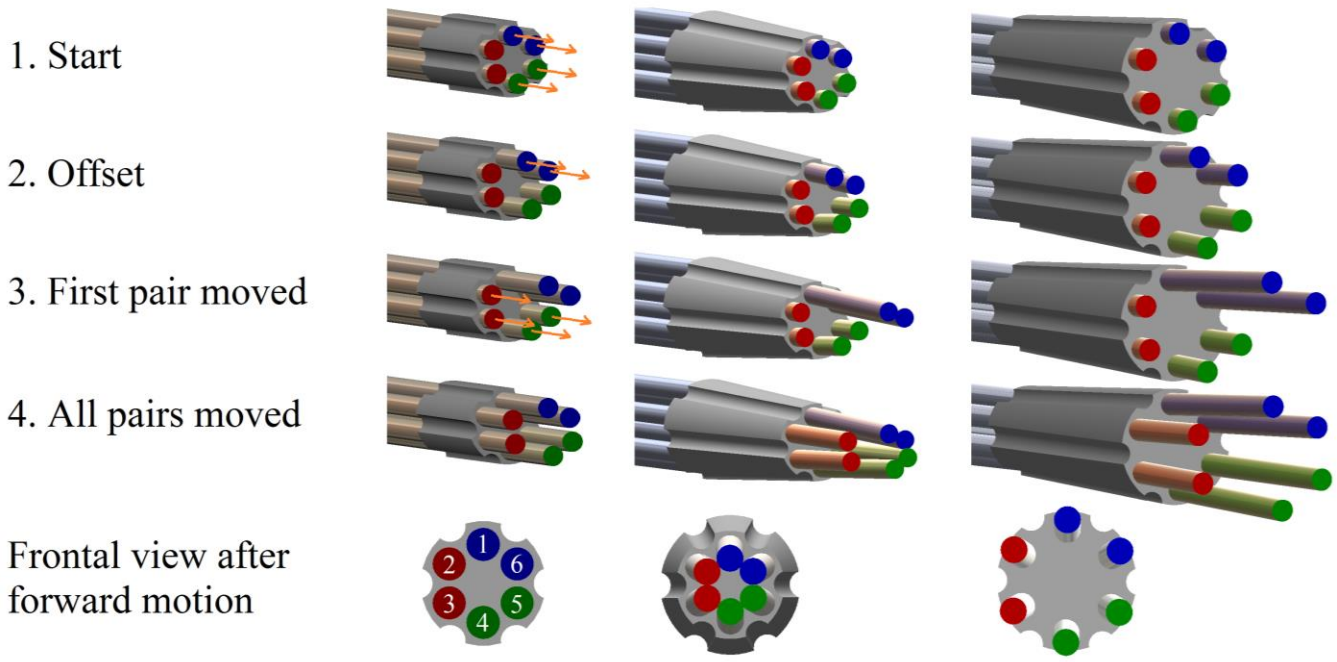

Figure 5: The three different ovipositor-inspired needle tips: cylindrical interlocking mechanism (left), conical interlocking mechanism that converges (middle) or diverges (right) the wires. The steps of the forward motion of the actuation cycle when the left side of the wires protrude are listed: 1. Initially, the wires are axially aligned; 2. The two pairs of wires are offset; 3. The first pair moves over a distance equal to the stroke; 4. All pairs have moved a distance equal to the stroke (note that the wires that are offset will always maintain at least the offset distance relative to the wires that are not offset). The frontal view of the interlocking mechanisms are shown after the full forward motion and the wires are numbered. The arrows (orange) indicate the movement direction of the respective wire. The hole of the central wire is not shown in any of the illustrations.

wires 1 and 6 when the left side protrudes; wires 1 and 2 when the right side protrudes) over a predefined distance (i.e., the stroke). Subsequently, the second pair of wires (i.e., wires 4 and 5 when the left side protrudes; wires 3 and 4 when the right side protrudes) is moved over a distance equal to the stroke. Next, analogously, the third and final pair (i.e., wires 2 and 3 when the left side protrudes; wires 5 and 6 when the right side protrudes, thus the pair that was not offset) is moved forward. After the movement of wire pairs, all six wires are retracted over the same distance simultaneously, causing the interlocking mechanism with the central wire to advance within the substrate.

The steering of the ovipositor-inspired needle with a conical interlocking mechanism depends on the tendency of the wires to move to the center (i.e., with the converging interlocking mechanism) or to the periphery (i.e., with the diverging interlocking mechanism). The asymmetry that is created by offsetting one side of the needle, depending on the desired steering direction, causes the wires of the needle to follow the trajectory cut by the preceding pairs of wires.

Equivalent to moving straight, the actuation cycles are repeated when steering until a precalculated number of cycles has been reached. The precalculated number is equal to the theoretical traveling distance divided by the stroke.

III. Materials and Methods

In order to test the ovipositor-inspired needle for its efficiency of advancing within a substrate as well as its steerability, two experiments were performed. Both experiments were conducted with ovipositor-inspired needle and each of the previously described interlocking mechanisms in order to compare their performance. In the first experiment (referred to as experiment 1) the penetration depth was measured when advancing the prototype within the substrate in a straight manner. In the second experiment (referred to as experiment 2) curvatures were created with the prototype using multiple actuation methods. Thus, in experiment 1 the losses of the forward motion of the ovipositor-inspired needle with the three interlocking mechanisms was determined; in experiment 2, the curvatures of the ovipositor-inspired needle produced with the three interlocking mechanisms were measured.

A. Experimental setup

For both experiments, an experimental setup was used that consists of an aluminum platform and an actuation unit, housing the motors and transmission (Figure 3b). The baseplate of the platform (ca. 405 x 101 mm) had a duct to guide a lightweight aluminum cross-shaped cart (max. dimensions: 200 x 100 mm, m = 39 g) in moving along a straight path. The base of the needle was fixed, while the cart, which held the gelatin phantom, was allowed to move towards the base. This allowed the needle to advance within in the substrate. The cart was fitted with two alignment ring holders, spaced 15 mm apart. A camera (Nikon D610 with AF-S NIKKOR 24–70 mm 1:2:8G ED lens) was positioned directly above the cart using a tripod to take a photograph of the initial insertion and final position of the needle (Figure 6). An

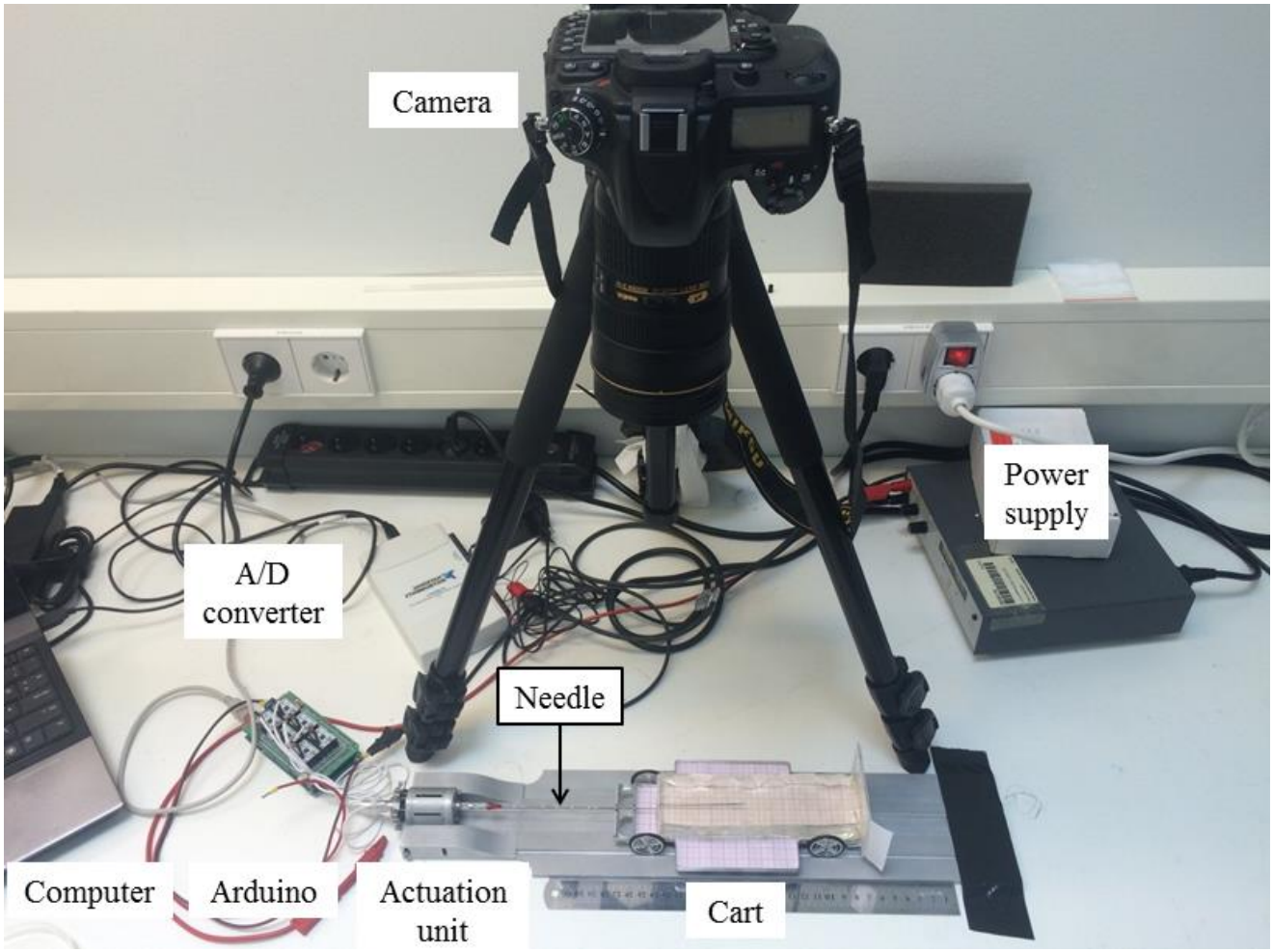

Figure 6: Overview of the experimental setup. The components are indicated (ultrasonic distance sensor not shown).

ultrasonic distance sensor (PIL 945-F4Y-AD-1C0-300E) was positioned at the side opposite of the actuation unit with respect to the baseplate. The analog signal output by the distance sensor was converted to a digital sensor using an A/D converter (NI USB-6211).

The gelatin phantoms were created by stirring hot (~70 °C) tap water and gelatin powder (Dr. Oetker Professional) in a measuring jug until a solution was formed. The solution was then poured into smaller containers (ca. 230 x 150 x 60 mm) and stored overnight (~16 hours) in a refrigerator (~5 °C). Before each measurement, a gelatin block (165 x 48 x 30 mm) was cut out of the containers using a rapid prototyped cutter to assure a consistent weight between measurements (200.0 ± 0.2 g).

B. Experimental design

Pilot experiments were conducted using the experimental setup and the ovipositor-inspired needle with the cylindrical interlocking mechanism. From these experiments, a constant forward speed of the wires equal to 1 mm/s and a gelatin concentration of 5 wt% was chosen. The 5-wt% gelatin concentration corresponds to brain tissue as described in Appendix B. In addition, a theoretical traveling distance equal to 120 mm was selected. A theoretical traveling distance of 120 mm is a compromise between the duration of a measurement and the amount of gelatin required (i.e., a deeper penetration requires a longer block of gelatin) that also adds to the weight of the cart. The pilot experiments showed that the cylindrical interlocking mechanism did not minimize bifurcation and was thus discarded. Only the two conical interlocking mechanisms were thus considered in experiments 1 and 2.

Experiment 1

1) *Hypotheses*: a) The converging interlocking mechanism design advances more within a gelatin substrate than a diverging interlocking mechanism design under the same conditions because the converging interlocking mechanism design is sleeker and thus suffers less from form drag.

b) Single wire actuation results in less slip than double wire actuation (and thus less losses or a higher energy conversion efficiency) because the axial insertion force of double wire actuation is larger, causing the reaction force of axial insertion force to overcome the static friction of the needle in the actuation cycle and the needle to be pushed out of the gelatin substrate.

2) *Dependent and independent variables*: The dependent variable was the traveling distance of the cart: an indirect measure of the distance the needle protrudes into the gelatin phantom. The independent variable was the number of wires

that were actuated simultaneously: single wire or double wire actuation and the type of interlocking mechanism (i.e., converging or diverging). There was no offset, and the stroke was equal to 4.0 mm.

3) *Experimental procedure*: Before each measurement, the needle was manually cleaned using lukewarm tap water. Next, each wire was inspected for a possible offset with respect to its adjacent wires. If so, the position of the wire was corrected using the code found in Appendix C. Subsequently, the needle would be inserted into and attached to the cart by fastening the two screws holding the alignment rings into place. Afterward the gelatin phantom was placed onto the cart. The ovipositor-inspired needle with converging interlocking mechanism was inserted approximately 35 mm (45 mm for the diverging interlocking mechanism due to its larger drag) into the phantom before the experiment commenced. The initial insertion was done by using the actuation for forward motion with a traveling distance of 30 mm, see Appendix D.

Once the needle was in place, the sensor and camera were turned on, and the code with predefined settings of steering direction, offset, and stroke was uploaded to the Arduino board and ran. See Appendix E for the Arduino code used to actuate the needle. In addition, the settings were extracted from the Arduino code using MATLAB R2014b and stored as a text file for future reference and validation of the settings in each measurements. See Appendix F the used MATLAB code. Both single wire and double wire actuation were repeated eight times in a randomized order with the converging and diverging interlocking mechanism. The type of interlocking mechanism was not part of the randomization as switching the interlocking mechanisms takes a considerable amount of time. After the needle was fully advanced within the substrate a photograph was taken. Hereafter, the gelatin was carefully removed by cutting it open to release the needle. As a final check, the wires were moved back and forth to inspect their functioning.

4) *Data analysis*: The raw data from the distance sensor was imported into MATLAB. Subsequently, the data was normalized by subtracting the value of the first data point from the all data points, to set the starting point to zero mm. The energy conversion efficiency was calculated by using

$$\text{efficiency} = \frac{\text{traveled dist.}}{\text{theoretical traveling dist.}} \quad (7)$$

where the theoretical traveling distance was equal to 120 mm during experiment 1 and 2.

Experiment 2

1) *Hypotheses*: a) The converging interlocking mechanism design produces a lower radius of curvature than a diverging interlocking mechanism design under the same conditions because the wires bifurcate less.

b) The offset of the wires causes the needle to produce a lower radius of curvature compared to less offsetting of the wires as the length of a wire protruding is increased relative to the interlocking mechanism, causing the needle to bend more.

TABLE II: EXPERIMENTAL CONDITIONS – EXPERIMENT 2

Condition	Offset [mm]	Stroke [mm]	Direction of protrusion
1	4.0	4.0	Left
2	6.0	4.0	Left
3	2.0	6.0	Left
4	6.0	6.0	Left
5	4.0	4.0	Right
6	6.0	4.0	Right
7	2.0	6.0	Right
8	6.0	6.0	Right

c) A larger stroke of the wires causes the needle to produce a lower radius of curvature compared to a small stroke of the wires as the length of a wire protruding is increased relative to the interlocking mechanism, causing the needle to bend more.

2) *Dependent and independent variables*: The dependent variable was the curvature of the needle after the movement was finished. The independent variables were the initial offset of the wires, the stroke, the steering direction, and the type of interlocking mechanism (i.e., converging or diverging). The offset was varied between 2.0, 4.0, and 6.0 mm. The stroke was varied between 4.0 and 6.0 mm. The steering direction was varied between left and right. The experimental conditions are shown in Table II.

3) *Experimental procedure*: The same experimental procedure as in experiment 1 was followed. All conditions were carried out eight times in a randomized order with the converging and diverging interlocking mechanism. Measurements that were not completed successfully due to the motors not actuating the wires correctly were repeated.

4) *Data analysis*: The photographs of the final position were cropped, imported into MATLAB, and processed to extract the curvature of the needle. The processing consisted of normalization, a conversion to black and white, and steps to dilate and erode the image and to remove the noise. The algorithm is shown in Appendix G. As some images were not processed correctly, these required altered steps, such as manual processing.

The extracted curvatures were further analyzed using an algorithm to fit a circle using nonlinear least squares Gauss-Newton method [68]. Using the algorithm, 100 iterations were performed with a tolerance 10^{-6} of to check for convergence. Subsequently, the direction of the curvatures was validated, and those of a needle steering in the opposite direction of what was to be expected were set to a negative value. Using the obtained radius of the fitted circle r, the curvature κ was calculated by

$$\kappa = (r)^{-1} \quad (8)$$

Furthermore, using the scaling factor that was determined by measuring the grid lines of an average of 10 randomly chosen images, the curvature was converted to 1/cm.

The Kolmogorov-Smirnov test was used to determine the distribution of the results. The Mann-Whitney test was used to compare the conditions among and between interlocking mechanisms for number of wires actuated, offset, stroke, and steering direction.

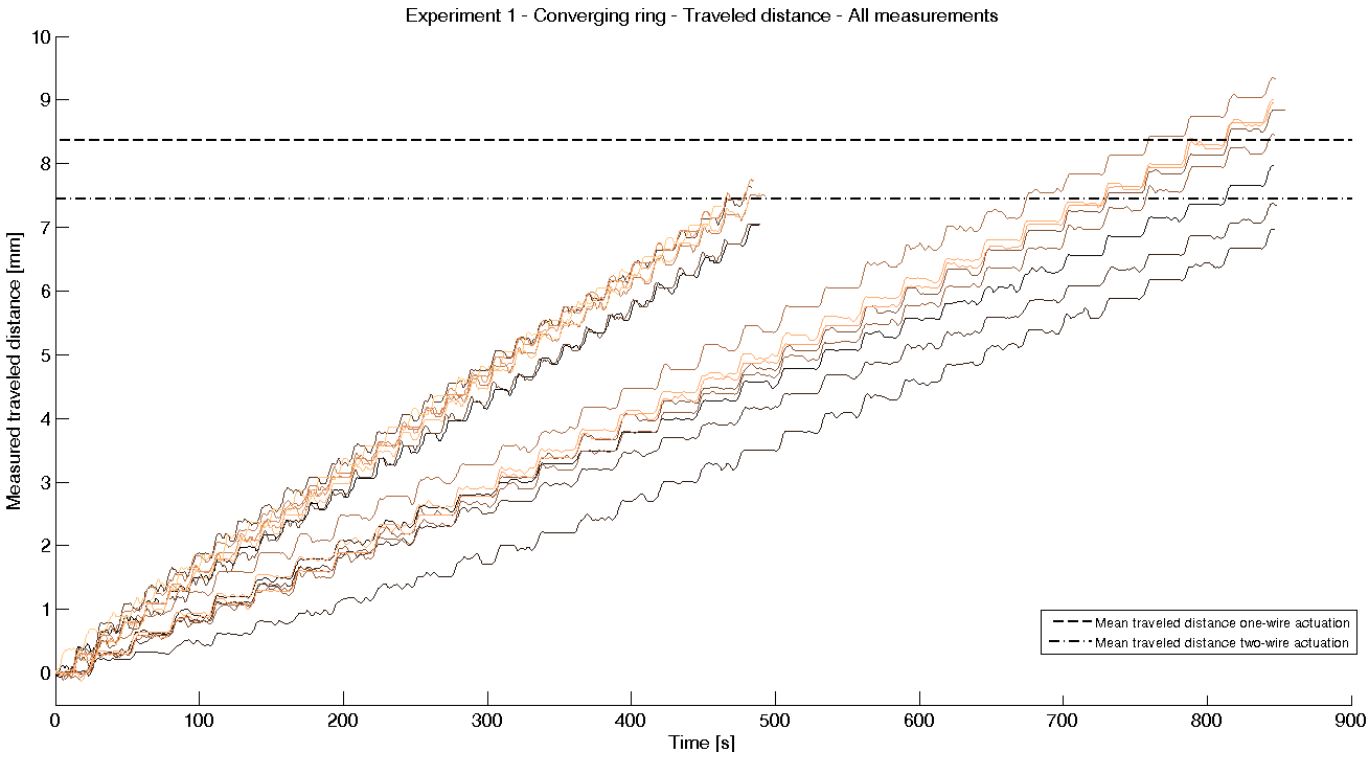

Figure 7: A plot of the traveled distance of the cart vs. time during a straight insertion of the ovipositor-inspired needle with a converging interlocking mechanism. In addition, the mean traveled distances for single and double wire actuation are indicated.

IV. Results

A. Experiment 1

In the case of the converging interlocking mechanism, the data shows that on average single wire actuation leads to less slip compared to double wire actuation and thus a more efficient ovipositor-inspired needle advancement within gelatin. This leads to a deeper penetration in these cases (M = 83.59 mm, SE = 3.02 mm) compared to double wire actuation (M = 74.41 mm, SE = 0.99 mm). The efficiency of single wire actuation (M = 0.70) is thus higher than that for double wire actuation (M = 0.62).There is less variability in actuating two wires (SD = 2.81 mm) than in actuating a single wire (SD = 8.54 mm). The traveled distance of each sample and the mean penetration depth for each condition are shown in Figure 7.

In case of the diverging interlocking mechanism, the data shows that on average single wire actuation leads to less slip compared with double wire actuation and thus a more efficient ovipositor-inspired needle advancement within gelatin. This leads to a deeper penetration in these cases (M = 70.24 mm, SE = 3.03 mm) compared to double wire actuation (M = 58.16 mm, SE = 3.85 mm). The efficiency of single wire actuation (M = 0.59) is thus higher than that for double wire actuation (M = 0.48)There is less variability in actuating a single wire (SD = 8.56 mm) than in actuating two wires (SD = 10.89 mm). The traveled distance of each sample and the mean penetration depth for each condition are shown in Figure 8.

The Kolmogorov-Smirnov test with the null hypothesis that the data from a group comes from a standard normal distribution does reject this null hypothesis among all four groups. In addition, as the sample size is small in experiment 1 and among each actuation method (n = 8), a nonparametric test is used. The Mann-Whitney test is used to compare single wire with the double wire actuation for the same ring and both conditions among both interlocking mechanisms. The penetration depth of the converging interlocking mechanism with single wire actuation was larger than double wire actuation (U = 49, p = 0.049, r = 0.77). Similarly, this was the case for the diverging interlocking mechanism (U = 48, p = 0.038, r = 0.75). When comparing the converging with the diverging interlocking mechanism, the converging interlocking mechanism significantly penetrates more than the diverging interlocking mechanism for single (U = 46, p = 0.021, r = 0.72) and double wire actuation (U = 36, p = 0.0002, r = 0.56).

B. Experiment 2

The measurements for the converging interlocking mechanism were initially completed successfully 61 out of 64 times. The three failed measurements were caused by motors not actuating the wires correctly and were repeated. As the curvature could not be extracted from a number of images, the following measurements were omitted. For conditions 1, 3, and 4, two measurements were omitted. For condition 2, four measurements were removed. For conditions 5, 6, 7, and 8 one measurement was omitted. Besides, the needle steered in a

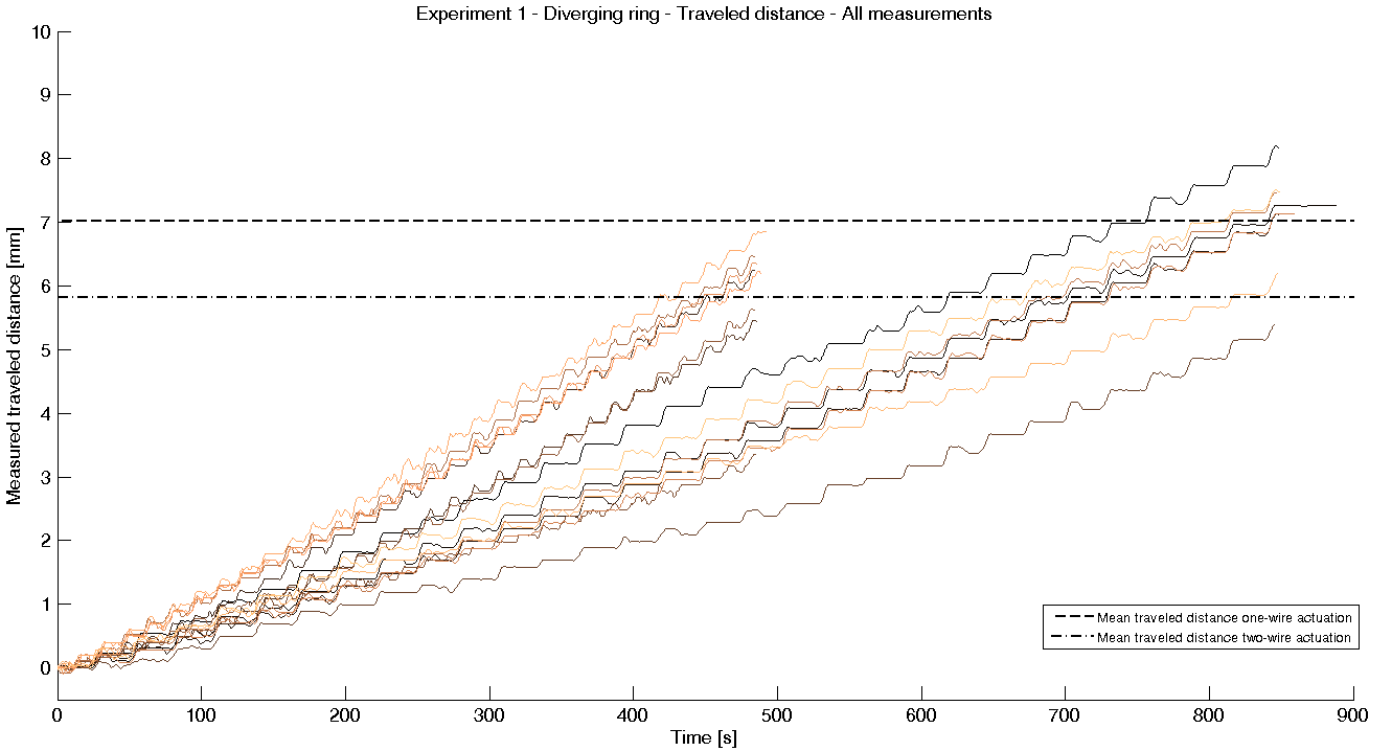

Figure 8: A plot of the traveled distance of the cart vs. time during a straight insertion of the ovipositor-inspired needle with a diverging interlocking mechanism. In addition, the mean traveled distances for single and double wire actuation are indicated.

direction opposite of what was to be expected in two measurements of condition 4, thus resulting in a negative curvature. Therefore, for two measurements of condition 4 the analyzed curvature was set to negative.

The absolute smallest achieved radius of curvature is equal to 35.899 cm for left side protruding and offset and stroke equal to 6 mm (i.e., condition 4). The largest achieved curvature is thus equal to 0.0279 cm^{-1}. On average, condition 2 (steering to left, offset and stroke equal to 6 and 4 mm) displayed the highest curvatures (M = 0.0142 cm^{-1}, SE = 0.005 cm^{-1}). The results are summarized in Table III and Figure 9.

The measurements for the diverging interlocking mechanism were initially completed successfully 55 out of 64 times. The nine failed measurements were caused by motors not actuating the wires completely and were repeated. As the curvature could not be extracted from a number of images, the following measurements were omitted. For conditions 2 and 4 one measurement was omitted. Besides, the needle steered in a direction opposite of what was to be expected in three measurements of condition 1, two measurements of condition 2, and one measurement of conditions 4 and 8, thus resulting in a negative curvature.

The smallest achieved radius of curvature is equal to 21.738 cm for the following condition: offset and stroke equal to 6.0 mm, right side protruding (i.e., condition 8). The largest achieved curvature is thus equal to 0.0460 cm^{-1}. On average, condition 5 (steering to right, offset and stroke equal to 4 mm) displayed the highest curvatures (M = 0.0226 cm^{-1}, SE = 0.002 cm^{-1}). The results are summarized in Table IV and Figure 10.

The Kolmogorov-Smirnov test with the null hypothesis that the data from a group comes from a standard normal distribution does reject this null hypothesis among all groups for the diverging interlocking mechanism and condition 5-8 for the converging interlocking mechanism. Data of condition 1-4 of the converging interlocking mechanism does come from a standard normal distribution according to the test (p_1 = 0.065, p_2 = 0.184, p_3 = 0.065, p_4 = 0.069). The results of the test are summarized in their respective tables (i.e., Table III and Table IV).

The Mann-Whitney test is used to compare the conditions that 1) vary by offset for each ring (i.e., four Mann-Whitney tests per ring); 2) vary by stroke for each ring (i.e., two tests per ring); 3) vary by direction for each ring (i.e., four tests per ring), and 4) vary by ring (i.e., eight tests in total). Only the significant results of the 28 tests are summarized in Table V. No significant differences in resulting curvatures are found when varying the offset, stroke, or direction for both interlocking mechanisms. However, for the diverging interlocking mechanism, steering to the right results in a significantly larger curvature than steering to the left for conditions 5 (U = 41, p = 0.003, r = 0.64), 6 (U = 35, p = 0.014, r = 0.63), and 7 (U = 46, p = 0.021, r = 0.72).

Last, when comparing the same conditions between both interlocking mechanisms, there is no significant difference in resulting curvatures, except for conditions 5 (U = 36, p = 0.021, r = 0.64) and 7 (U = 35, p = 0.014, r = 0.63): steering the needle with the diverging interlocking mechanism leads to significantly larger curvatures in these conditions.

TABLE III: SUMMARY OF RESULTS – EXPERIMENT 2 – CONVERGING INTERLOCKING MECHANISM

	Condition[a]	Sample size	Mean curvature [10^{-3}/cm]	SE [10^{-3}/cm]	Maximum curvature [10^{-3}/cm]	Smallest bending radius [cm]	*Kolmogorov-Smirnov test*	
							Normality	p
1	O4S4L	6	9.857	1.899	15.506	64.490	Yes	0.065
2	O6S4L	4	14.247	4.512	24.645	40.577	Yes	0.184
3	O2S6L	6	6.620	1.698	13.562	73.735	Yes	0.065
4	O6S6L	6	8.231	5.869	27.856	35.899	Yes	0.069
5	O4S4R	7	14.191	1.955	23.854	41.921	No	0.036
6	O6S4R	7	11.412	2.540	24.394	40.994	No	0.037
7	O2S6R	7	11.014	1.669	17.786	56.225	No	0.037
8	O6S6R	7	7.106	1.182	13.064	76.547	No	0.038

[a]O: offset, S: stroke, numbers indicating the amount in mm, L/R indicates the side of the needle that protrudes

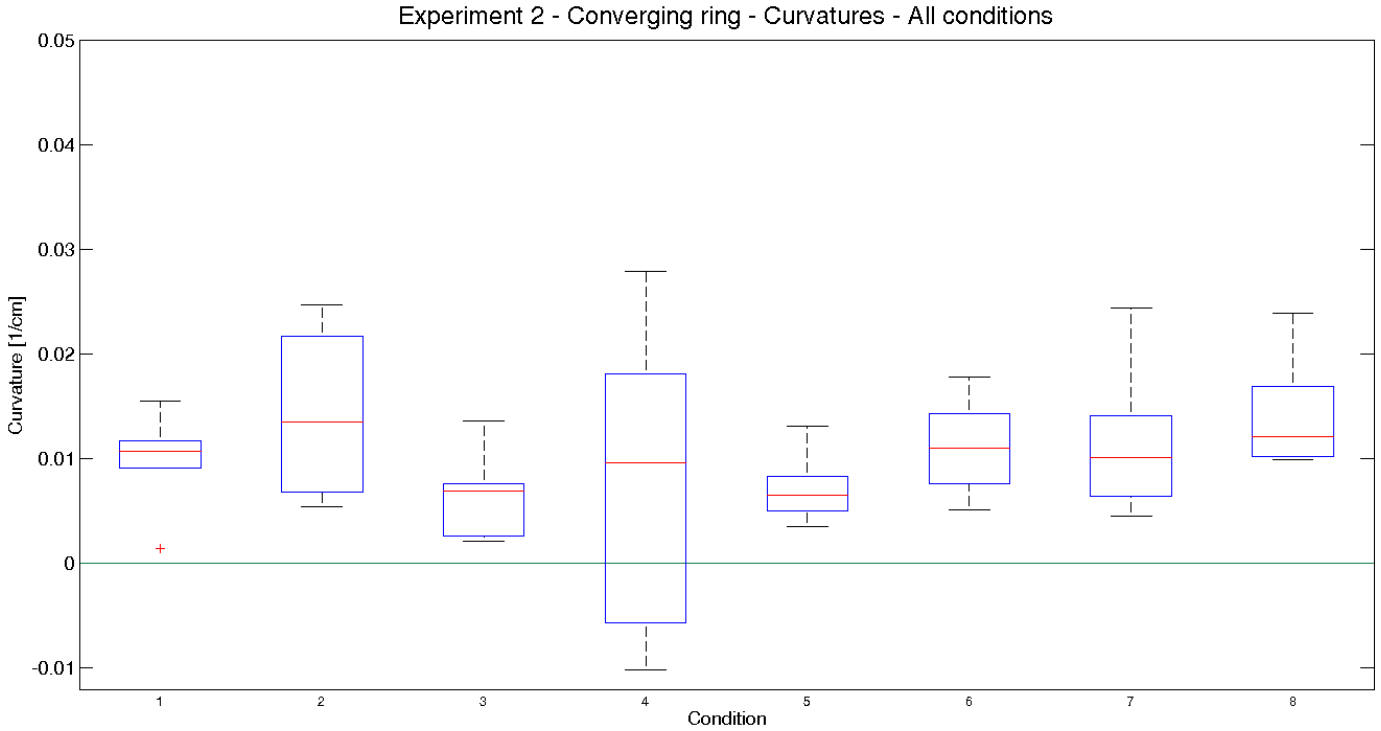

Figure 9: Box plot of the achieved curvatures produced by ovipositor-inspired needle with the converging interlocking mechanism per experimental condition. Indicated are the median (red), the top and bottom of each box (blue) depicting the 25th and 75th percentiles of the samples, the whiskers (black) indicating the most extreme data not considered outliers, and the outlier (red + sign).

TABLE IV: SUMMARY OF RESULTS – EXPERIMENT 2 – DIVERGING INTERLOCKING MECHANISM

	Condition[a]	Sample size	Mean curvature [10^{-3}/cm]	SE [10^{-3}/cm]	Maximum curvature [10^{-3}/cm]	Smallest bending radius [cm]	*Kolmogorov-Smirnov test*	
							Normality	p
1	O4S4L	8	5.136	3.493	27.194	36.773	No	0.023
2	O6S4L	7	5.834	2.436	16.904	59.159	No	0.389
3	O2S6L	8	9.459	2.051	15.553	64.296	No	0.224
4	O6S6L	7	13.804	4.213	29.192	34.256	No	0.390
5	O4S4R	8	22.577	2.445	31.643	31.603	No	0.020
6	O6S4R	8	17.150	2.806	25.829	38.717	No	0.022
7	O2S6R	8	16.851	1.239	21.902	45.658	No	0.021
8	O6S6R	8	17.277	6.734	46.002	21.738	No	0.026

[a]O: offset, S: stroke, numbers indicating the amount in mm, L/R indicates the side of the needle that protrudes

TABLE V: SUMMARY OF SIGNIFICANT RESULTS – EXPERIMENT 2 – MANN-WHITNEY TEST

Comparing Condition		Variable[a]	U	p	Effect size r	Conclusion
1-5	Diverging	D	41	0.003	0.64	Significant difference between condition 1-5
2-6	Diverging	D	35	0.014	0.63	Significant difference between condition 2-6
3-7	Diverging	D	46	0.021	0.72	Significant difference between condition 3-7
5-5	Conv./Div.	R	36	0.021	0.64	Significant difference between converging/diverging condition 5
7-7	Conv./Div.	R	35	0.014	0.63	Significant difference between converging/diverging condition 7

[a]O: offset, S: stroke, D: direction, R: ring

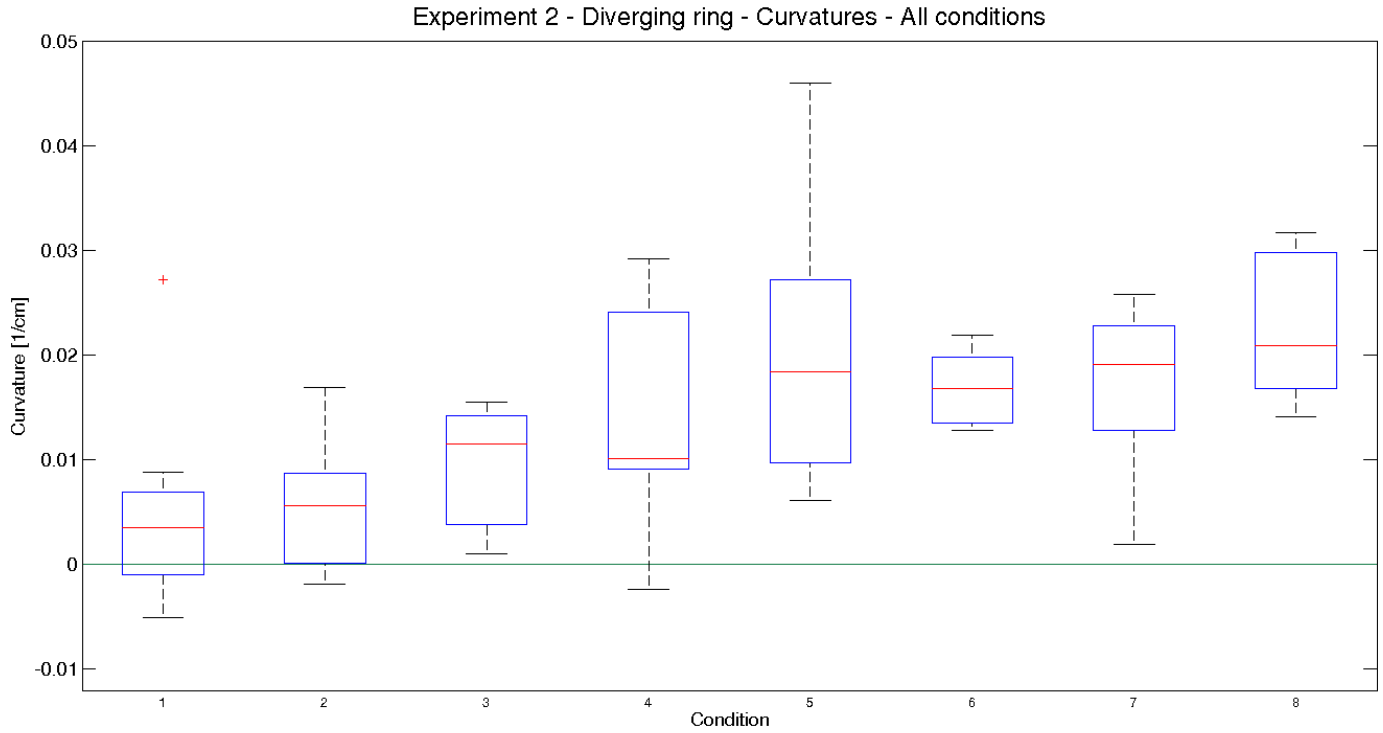

Figure 10: Box plot of the achieved curvatures produced by ovipositor-inspired needle with the diverging interlocking mechanism per experimental condition. Indicated are the median (red), the top and bottom of each box (blue) depicting the 25th and 75th percentiles of the samples, the whiskers (black) indicating the most extreme data not considered outliers, and the outlier (red + sign).

V. Discussion

In this thesis, a steerable needle prototype inspired by the ovipositor of a parasitoid wasp was presented. The ovipositor-inspired needle was fitted with two different interlocking mechanisms in order to control the bifurcation of the wires and to minimize the radius of curvature, i.e., to increase steerability. The performance of the two interlocking mechanisms was established in experiment 1 that tested the energy conversion efficiency when advancing within a gelatin substrate, and experiment 2 that tested for the amount of steering.

A. Experiment 1

The results are in line with the hypothesis that using the ovipositor-inspired needle with the converging interlocking mechanism leads to a significantly deeper penetration and thus higher energy conversion efficiency than the diverging interlocking mechanism. The difference in depth can be explained by the increased amount of form drag in the case of the diverging interlocking mechanism. The equation for drag force is given by

$$F_D = \frac{1}{2}\rho v^2 C_D A \qquad (9)$$

where F_D is the drag force, ρ the density of the fluid, v the speed of the object, A the cross sectional area, and C_D the drag coefficient. The drag force for the diverging interlocking mechanism is larger due to its shape having a larger drag coefficient as the remaining variables in the equation are equal among both interlocking mechanisms.

Single wire actuation leads to less slip in both interlocking mechanisms compared to double wire actuation. However, the required time for the needle to penetrate the substrate over the same distance is about 2·0.62/0.70 = 1.77 times as high for single wire actuation with the converging interlocking mechanism, and 2·0.48/0.59 = 1.63 times as high with the diverging interlocking mechanism when considering the energy conversion efficiency. Although the total procedure time might be less relevant in, for example, brachytherapy as the majority of its costs are concerned with intramural care [69].

Compared to previous work [39, 70], the current ovipositor-inspired needle has an efficiency that is higher than 0.3 (i.e., ranging from 0.48 to 0.70 depending on the mode of actuation and the type of interlocking mechanism). A previously reported prototype using a similar mode of actuation, had an efficiency of approximately 0.3. The prototype consisted of four parts totaling a diameter of 2 mm and was inserted into an 8-wt% gelatin phantom using single wire actuation with a speed of 4 mm/s [70]. In addition, the stroke was set to 4 mm. Compared to the previously reported prototype, the ovipositor-inspired needle exhibited a more efficient single wire actuation (i.e., 0.59 for the converging and 0.70 for the diverging interlocking mechanism) which could be attributed to the lower diameter of the actuated elements (i.e., wires of ⌀0.25 mm in the ovipositor-inspired needle compared to ⌀0.5 mm in the previous prototype) and the lower speed (i.e., 1 mm/s vs. 4 mm/s); The axial insertion force increases with needle diameter [71] and insertion speed [72, 73], potentially leading to a lower energy conversion efficiency. In addition, the used

gelatin phantoms (i.e., 5-wt% vs. 8-wt%) differed in stiffness which could further explain the difference. Compared to a previous iteration of the ovipositor-inspired needle having a cylindrical interlocking mechanism (4 wt% gelatin, insertion speed: 2 mm/s, stroke: 4 mm), the ovipositor-inspired needle exhibited a lower efficiency for single wire (i.e., 0.79 vs. 0.59 and 0.70) and double wire actuation (i.e., 0.67 vs. 0.48 and 0.62) [39]. The difference could be explained by the lower amount of form drag of a cylindrical compared to a conical interlocking mechanism. The effect of a larger form drag is thus potentially stronger than the effect of a higher insertion speed, which increases the peak axial insertion force [72, 73].

B. Experiment 2

The smallest achieved radius of curvature for the converging interlocking mechanism was in the condition where the stroke and offset were equal to 6 mm when the left side was protruding (i.e., r = 35.899 cm) and for the diverging interlocking mechanism needle when the right side was protruding (i.e., r = 21.738 cm). The ovipositor-inspired needle with the diverging interlocking mechanism produced a significantly larger curvature when steering to the right compared to the left in three out of four conditions. The inconsistency could be caused by a bias in the wires of the needle, although the effect was not present in the ovipositor-inspired needle with the converging interlocking mechanism when using the same wires. Therefore, it is likely that the difference between steering directions is caused by an effect in the diverging interlocking mechanism itself or in its interaction with the wires. For example, as the ovipositor-inspired needle was used with the diverging interlocking mechanism after the converging interlocking mechanism, the holes of interlocking mechanism could not have had an equal diameter due to wear. As a result, this allows the wires inside the diverging interlocking mechanism to bend in an asymmetric manner, causing a difference between the two steering directions. In addition, the interlocking mechanism could have been rotated axially, causing the outer wires to not be aligned with the base of the needle and their respective motors. Consequently, the discrepancy between the base and tip of the needle could cause torsion inside the wires influencing their movement.

For two out of eight conditions, the steerability of the ovipositor-inspired needle with the diverging interlocking mechanism is significantly larger, while the curvature does not differ significantly between the interlocking mechanisms in the remaining conditions. This is not in line with the hypothesis that the converging interlocking mechanism design produces a lower radius of curvature than the diverging design. A possible cause for the difference in resulting curvatures between the two interlocking mechanisms could be that steering costs less energy for the diverging interlocking mechanism as part of the wires already have a tendency to steer towards a certain direction, more so than with the converging interlocking mechanism design. Nonetheless, the advantage of having part of the wire move to the desired steering direction could be canceled out as the interlocking

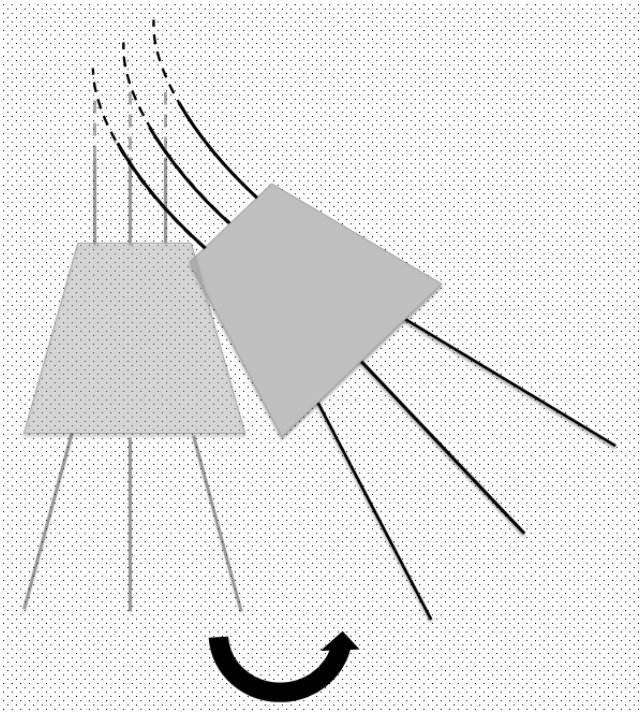

Figure 11: Illustration of how the diverging interlocking mechanism (in gray) might tilt to one side when minimizing the total potential energy. The black lines indicate the wires and the dashed lines indicate that the wires continue toward the needle base. The tip is pointing downwards.

mechanism is symmetric, though not during the actuation at all times. Moreover, the increased initial insertion depth could also play a role as it could cause less slip in the starting phase of the needle penetration, thereby losing less energy that could be used for steering instead. Furthermore, the diverging interlocking mechanism might tilt to one side when steering towards a certain direction, such as depicted in Figure 11, due to its shape as the interlocking mechanism tries to minimize the total potential energy. Last, another effect could be that the wires that were actuated at the start exert a force on the inner wall of the diverging interlocking mechanism, also causing it to tilt due to the opposite reaction force. In summary, the hypothesis of the converging interlocking mechanism leading to larges curvatures due to less bifurcation is rejected.

Compared to the previous iteration [39], the ovipositor-inspired needle with the diverging interlocking mechanism outperformed its predecessor in terms of maximum average curvature (i.e., κ = 0.0226 cm^{-1} vs. κ = 0.0184 cm^{-1}). The experimental condition was similar in terms of offset (i.e., 4 mm vs. 3.6 mm) and steering direction (to the right), but the stroke was lower (i.e., 4 mm vs. 2 mm). In contrast, the ovipositor-inspired needle with the converging interlocking mechanism exhibits worse steerability (i.e., maximum average κ = 0.0142 cm^{-1}) than the previous iteration in its most comparable condition (offset and stroke equal to 4 mm, steering to the right). Nonetheless, the results might not be comparable due to the limited conclusiveness of the previous work [39].

Compared to the results from literature as seen in Table I, the lowest average radius of curvature for the ovipositor-

inspired needle with the diverging interlocking mechanism (i.e., r = 44.23 cm) is high; The lowest reported radius of curvature in literature is 33.3 cm, although this needle was based on a bevel tip wire (⌀0.52 mm). The lowest reported value is 3.4 cm, for a pre-bent bevel tip needle (⌀0.58 mm). In general, as observed in Table I, needles exhibiting the highest steerability have a diameter smaller than the ovipositor-inspired needle. Most of the pre-bent bevel tip needles also demonstrate lower radii of curvature than the ovipositor-inspired needle, in line with observations from literature [42, 46, 49, 55-57].

The method of fitting a circle to a curve involves at least the following assumptions: 1) the needle travels along a plane during the whole insertion sequence (i.e., does not move in more than 1 direction), and 2) the curvature is constant along the trajectory. However, movement in the vertical plane was present: during experiment 2 with the converging interlocking mechanism, the ovipositor-inspired needle moved down 13 times and up 15 times. The ovipositor-inspired needle with the diverging interlocking mechanism moved down 23 times and up 11 times during experiment 2. Although the undesired movement in other planes was mostly occurring at the end of the motion, a cause could have been the initial insertion of the ovipositor-inspired needle: a minor deviation from a straight initial insertion could cause a major effect as the needle advances further within the substrate. Another aspect is that the curvature of the ovipositor-inspired needle could be approximated by a polynomial instead of a circle with a fixed radius (or a circular segment). Nonetheless, changing the mathematical approximation of the curvature makes comparing the needle between conditions and among the interlocking mechanisms complicated, as there would not be a single comparable number (e.g., radius of curvature or curvature). Furthermore, the results reported in literature are either all radius of curvature or curvature itself, thus requiring either of the two values for comparison in any case.

C. Limitations

A limitation of this work is the fact that only curvatures in 2D are considered. The measurement of the curvatures produced by the ovipositor-inspired needle would be more accurate and precise when the curvatures could be measured in 3D by, for example, using a second camera setup. In this way, the movement of the needle in other planes is also considered. Consequently, the amount of necessary care when initially inserting the needle straightly into the gelatin substrate is limited, possibly making the alignment rings and their holders redundant as the initial insertion would not have to be consistent. Besides, when implementing a more precise system that directly measures the position of the needle using, for example, fiber Bragg gratings [74], the constant error involved with taking photographs using the current setup would be solved: The grid background on the base of the cart (that is positioned lower than the needle itself) introduces a deviation when attempting to measure the curvature of a needle that is positioned above it. However, the error probably has a minor impact on the results, and most comparable studies also suffer from the same issue. See for example ref. [50], [51], and [18]. Nonetheless, researching the effects of the insertion on the resulting curvature would be useful to quantify the deviation.

During the pilot experiments with the ovipositor-inspired needle the transmission of individual wires sometimes jammed. The transmission of a wire getting stuck was much more prominent when the needle was inserted into higher concentrations of gelatin. The exact reason(s) for the (infrequent) occurrence are unknown, as the transmission was always kept well-lubricated. A possible hypothesis is that the motors driving the wires are possibly not powerful enough, although this seems unlikely when considering their specifications. Another possibility is the transmission itself: The transmission consists of a housing with a V-shape for every outer wire that receives another, yet smaller V-shaped slider attached to the respective wire. The sliders could get wedged due to vibrations present in the transmission. Whenever a slider would be stuck, the motor would not be able to overcome static friction and the wires could get stuck. A redesign of the transmission could therefore benefit the ovipositor-inspired needle by being less prone to internal and external vibrations.

Both types of interlocking mechanisms sometimes were not able to move the needle in a perfectly straight manner, but lead to a deflection of a few millimeters at the end of the insertion. Therefore, a control system incorporating feedback about the position of the needle would highly benefit the movement in a straight line. In addition, feedback control would also solve the cumbersome initial calibration of the wires such that they are all aligned laterally. Moreover, it would allow for a more flexible control as the actuation routine could be changed during the movement.

Some minor drawbacks of the current design include the use of the support rings that keep shifting back and forth during the movement of the needle. This effect needs almost constant observation and manual adjustment in order to prevent buckling and jamming of the wires. The manual movement of the support rings could have influenced the measurements of the ovipositor-inspired needle as the vibrations at the base could have caused vibrations at the tip, thereby affecting the path of the needle. In addition, the use of Arduino to control the motors severely limited real-time control over the needle actuation. As preprogrammed software has to be loaded onto the board where it is subsequently executed, the user of the needle can merely start and stop the execution without any adjustments ‘on the fly’.

D. Future work

Future iterations of the ovipositor-inspired needle to further decrease the radius of curvatures it produces could include decreasing the total number of wires to reduce the needle diameter. In addition, this possibly speeds up the insertion as fewer wires are actuated during a step. However, the benefit(s) of a faster needle insertion remains unknown and depends on the use case. Moreover, altering the design of the ovipositor-inspired needle such that the interlocking mechanism is omitted, possibly in combination with the

removal of the central wire, could lead to higher curvatures and a smaller overall diameter as the interlocking mechanism could inhibit steering of the wires. When maintaining the interlocking mechanism, it could also be altered such that it does not limit the steering of the ovipositor-inspired needle. For example, this could be achieved by creating a flexible interlocking mechanism or one that could hinge. Hinging could for example be achieved by using compliant geometries based on origami [75] as compliant mechanisms reduce backlash and friction found in traditional joints [76]. Another beneficial design change could be the use of an interlocking mechanism that is not fixed, but one that is able to slide back and forth freely. This would allow the outer wires to be kept together, and thus to maintain the integrity of the ovipositor-inspired needle, while the central wire that currently acts as a fixation for the interlocking mechanism could be omitted. It is important when using a movable interlocking mechanism that it cannot rotate axially, as this would cause the wires to not be aligned, possibly resulting in torsion inside the wires. A design solution could be the use of protuberances on the outer wires to move the interlocking mechanism accordingly.

The experimental setup would benefit from a fundamental design change. By letting the actuation unit move instead of the cart, some issues can be solved. These issues include the cutting and weighing of the gelatin, which is taking up a considerable amount of time when preparing a measurement. In addition, it is more convenient when taking photographs as the position of the gelatin block is fixed in the case of the actuation unit moving instead of the cart. Consequently, as the photographs would always be in focus, the image processing benefits.

VI. Conclusion

Two conical interlocking mechanism designs were tested on a novel steerable needle prototype: the ovipositor-inspired needle. The first interlocking mechanism design made the wires converge (i.e., converging interlocking mechanism), while the second design made the wire diverge (i.e., diverging interlocking mechanism). The energy conversion efficiency of the penetration of the ovipositor-inspired needle within a gelatin substrate was lower for the diverging interlocking mechanism than for the converging interlocking mechanism, but the importance of exhibiting an efficient forward motion is not well established. Single wire actuation lead to significantly larger penetration depths than double wire actuation for both interlocking mechanism designs. Compared to the previous iteration of the ovipositor-inspired needle that was fitted with a cylindrical interlocking mechanism, the energy conversion efficiency of the ovipositor-inspired needle with the two conical interlocking mechanism designs was lower, most likely due to the increased form drag.

The ovipositor-inspired needle with a converging interlocking mechanism was able to produce a maximum average curvature of 0.0142 cm^{-1}, while the prototype with the diverging interlocking mechanism was able to produce a maximum average curvature of 0.0226 cm^{-1}. Compared to the previous iteration of the ovipositor-inspired needle that was fitted with a cylindrical interlocking mechanism (producing a maximum average curvature of 0.0184 cm^{-1}), the diverging interlocking mechanism increased the steerability of the ovipositor-inspired needle design. Conclusively, the ovipositor-inspired needle with a diverging interlocking mechanism is the most desired to explore further in future iterations of the ovipositor-inspired steerable needle design.

Acknowledgment

This work has been supported by the Dutch Technology Foundation STW (Project 12712), which is part of the Netherlands Organization for Scientific Research (NWO), and is partly funded by the Ministry of Economic Affairs.
D. Kreeft thanks Menno Lageweg from DEMO (Dienst Elektronische en Mechanische Ontwikkeling) for fabricating the prototype and his input on the design as well as A. van Dijke and D.J. van Gerwen for their help.

References

[1] R. J. Roesthuis, M. Abayazid, and S. Misra, "Mechanics-based model for predicting in-plane needle deflection with multiple bends," in *Biomedical Robotics and Biomechatronics (BioRob), 2012 4th IEEE RAS & EMBS International Conference on*, 2012, pp. 69-74.

[2] S. Misra, K. B. Reed, B. W. Schafer, K. T. Ramesh, and A. M. Okamura, "Observations and models for needle-tissue interactions," in *Robotics and Automation, 2009. ICRA'09. IEEE International Conference on*, 2009, pp. 2687-2692.

[3] J. H. Youk, E. K. Kim, M. J. Kim, J. Y. Kwak, and E. J. Son, "Analysis of false-negative results after US-guided 14-gauge core needle breast biopsy," *Eur Radiol*, vol. 20, pp. 782-9, Apr 2010.

[4] A. Volpe, J. R. Kachura, W. R. Geddie, A. J. Evans, A. Gharajeh, A. Saravanan, *et al.*, "Techniques, safety and accuracy of sampling of renal tumors by fine needle aspiration and core biopsy," *J Urol*, vol. 178, pp. 379-86, Aug 2007.

[5] S. Pesek, T. Ashikaga, L. E. Krag, and D. Krag, "The false-negative rate of sentinel node biopsy in patients with breast cancer: a meta-analysis," *World J Surg*, vol. 36, pp. 2239-51, Sep 2012.

[6] J. E. Dawson, T. Wu, T. Roy, J. Y. Gu, and H. Kim, "Dose effects of seeds placement deviations from pre-planned positions in ultrasound guided prostate implants," *Radiother Oncol*, vol. 32, pp. 268-70, Sep 1994.

[7] P. L. Roberson, V. Narayana, D. L. McShan, R. J. Winfield, and P. W. McLaughlin, "Source placement error for permanent implant of the prostate," *Med Phys*, vol. 24, pp. 251-7, Feb 1997.

[8] G. Wan, Z. Wei, L. Gardi, D. B. Downey, and A. Fenster, "Brachytherapy needle deflection evaluation and correction," *Med Phys*, vol. 32, pp. 902-9, Apr 2005.

[9] S. Nath, Z. Chen, N. Yue, S. Trumpore, and R. Peschel, "Dosimetric effects of needle divergence in prostate seed implant using 125I and 103Pd radioactive seeds," *Medical physics*, vol. 27, pp. 1058-1066, 2000.

[10] N. N. Stone, J. Roy, S. Hong, Y. C. Lo, and R. G. Stock, "Prostate gland motion and deformation caused by needle placement during brachytherapy," *Brachytherapy*, vol. 1, pp. 154-60, 2002.

[11] H. Willschke, A. Bösenberg, P. Marhofer, S. Johnston, S. Kettner, O. Wanzel, *et al.*, "Ultrasonography-guided rectus sheath block in paediatric anaesthesia—a new approach to an old technique," *British journal of anaesthesia*, vol. 97, pp. 244-249, 2006.

[12] M. Scali, T. P. Pusch, P. Breedveld, and D. Dodou, "Needle-like instruments for steering through solid organs: a review of the scientific and patent literature," *Journal of Engineering in Medicine*, 2016.

[13] I. Elgezua, Y. Kobayashi, and M. G. Fujie, "Survey on Current State-of-the-Art in Needle Insertion Robots: Open Challenges for Application in Real Surgery," *Procedia CIRP*, vol. 5, pp. 94-99, 2013.

[14] R. Alterovitz, K. Goldberg, and A. M. Okamura, "Planning for steerable bevel-tip needle insertion through 2D soft tissue with obstacles," in *Robotics and Automation, 2005. ICRA 2005. Proceedings of the 2005 IEEE International Conference on*, 2005, pp. 1640-1645.

[15] N. Abolhassani and R. Patel, "Deflection of a flexible needle during insertion into soft tissue," in *Engineering in Medicine and Biology Society, 2006. EMBS'06. 28th Annual International Conference of the IEEE*, 2006, pp. 3858-3861.

[16] Y. Wang, R. K. Chen, B. L. Tai, P. W. McLaughlin, and A. J. Shih, "Optimal needle design for minimal insertion force and bevel length," *Med Eng Phys*, vol. 36, pp. 1093-100, Sep 2014.

[17] L. Tang, Y. Chen, and X. He, "Magnetic force aided compliant needle navigation and needle performance analysis," in *Robotics and Biomimetics, 2007. ROBIO 2007. IEEE International Conference on*, 2007, pp. 612-616.

[18] S. Okazawa, R. Ebrahimi, J. Chuang, S. E. Salcudean, and R. Rohling, "Hand-held steerable needle device," *Mechatronics, IEEE/ASME Transactions on*, vol. 10, pp. 285-296, 2005.

[19] P. Sears and P. Dupont, "A steerable needle technology using curved concentric tubes," in *Intelligent Robots and Systems, 2006 IEEE/RSJ International Conference on*, 2006, pp. 2850-2856.

[20] P. J. Swaney, A. W. Mahoney, A. A. Remirez, E. Lamers, B. I. Hartley, R. H. Feins, *et al.*, "Tendons, concentric tubes, and a bevel tip: Three steerable robots in one transoral lung access system," in *Robotics and Automation (ICRA), 2015 IEEE International Conference on*, 2015, pp. 5378-5383.

[21] R. J. Webster III, A. M. Okamura, and N. J. Cowan, "Toward active cannulas: Miniature snake-like surgical robots," in *Intelligent Robots and Systems, 2006 IEEE/RSJ International Conference on*, 2006, pp. 2857-2863.

[22] N. J. Van de Berg, J. Dankelman, and J. J. Van den Dobbelsteen, "Design of an actively controlled steerable needle with tendon actuation and FBG-based shape sensing," *Med Eng Phys*, vol. 37, pp. 617-22, Jun 2015.

[23] L. B. Kratchman, M. M. Rahman, J. R. Saunders, P. J. Swaney, and R. J. Webster III, "Toward robotic needle steering in lung biopsy: a tendon-actuated approach," in *SPIE Medical Imaging*, 2011, pp. 79641I-79641I-8.

[24] D. P. Losey, P. A. York, P. J. Swaney, J. Burgner, and R. J. Webster, "A flexure-based wrist for needle-sized surgical robots," in *SPIE Medical Imaging*, 2013, pp. 86711G-86711G-9.

[25] K. B. Reed, A. Majewicz, V. Kallem, R. Alterovitz, K. Goldberg, N. J. Cowan, *et al.*, "Robot-Assisted Needle Steering," *IEEE Robot Autom Mag*, vol. 18, pp. 35-46, Dec 8 2011.

[26] R. J. Webster III, J. Memisevic, and A. M. Okamura, "Design considerations for robotic needle steering," in *Robotics and Automation, 2005. ICRA 2005. Proceedings of the 2005 IEEE International Conference on*, 2005, pp. 3588-3594.

[27] S. Y. Ko and F. Rodriguez y Baena, "Toward a miniaturized needle steering system with path planning for obstacle avoidance," *IEEE Trans Biomed Eng*, vol. 60, pp. 910-7, Apr 2013.

[28] K. B. Reed, A. M. Okamura, and N. J. Cowan, "Modeling and control of needles with torsional friction," *IEEE Trans Biomed Eng*, vol. 56, pp. 2905-16, Dec 2009.

[29] J. P. Swensen, M. Lin, A. M. Okamura, and N. J. Cowan, "Torsional dynamics of steerable needles: modeling and fluoroscopic guidance," *IEEE Trans Biomed Eng*, vol. 61, pp. 2707-17, Nov 2014.

[30] J. Vincent and M. King, "The mechanism of drilling by wood wasp ovipositors," *Biomimetics (USA)*, 1995.

[31] L. Frasson, S. Y. Ko, A. Turner, T. Parittotokkaporn, J. F. Vincent, and F. Rodriguez y Baena, "STING: a soft-tissue intervention and neurosurgical guide to access deep brain lesions through curved trajectories," *Proceedings of the Institution of Mechanical Engineers, Part H: Journal of Engineering in Medicine*, vol. 224, pp. 775-788, 2010.

[32] L. Frasson, F. Ferroni, S. Y. Ko, G. Dogangil, and F. Rodriguez y Baena, "Experimental evaluation of a novel steerable probe with a programmable bevel tip inspired by nature," *J Robot Surg*, vol. 6, pp. 189-97, Sep 2012.

[33] M. J. Oldfield, C. Burrows, J. Kerl, L. Frasson, T. Parittotokkaporn, F. Beyrau, *et al.*, "Highly resolved strain imaging during needle insertion: Results with a novel biologically inspired device," *J Mech Behav Biomed Mater*, vol. 30, pp. 50-60, Feb 2014.

[34] C. Burrows, R. Secoli, and F. Rodriguez y Baena, "Experimental characterisation of a biologically inspired 3D steering needle," in *Control, Automation and Systems (ICCAS), 2013 13th International Conference on*, 2013, pp. 1252-1257.

[35] A. Leibinger, M. J. Oldfield, and Y. B. F. Rodriguez, "Minimally disruptive needle insertion: a biologically inspired solution," *Interface Focus*, vol. 6, p. 20150107, Jun 6 2016.

[36] M. J. Oldfield, A. Leibinger, T. E. T. Seah, and Y. B. F. Rodriguez, "Method to reduce target motion through needle–tissue interactions," *Annals of biomedical engineering*, vol. 43, pp. 2794-2803, 2015.

[37] S. Y. Ko, B. L. Davies, and F. R. y Baena, "Two-dimensional needle steering with a "Programmable Bevel" inspired by nature: modeling preliminaries," in *Intelligent Robots and Systems (IROS), 2010 IEEE/RSJ International Conference on*, 2010, pp. 2319-2324.

[38] M. Scali, T. P. Pusch, P. Breedveld, and D. Dodou, "Ovipositor-inspired steerable needle: design and preliminary study (in press)," 2017.

[39] T. P. Pusch, "From the Wasp Ovipositor to a 3D Steerable Needle for Solid-Tissue Interventions," MSc, Biomechanical Engineering, Delft University of Technology, 2016.

[40] S. Misra, K. B. Reed, A. S. Douglas, K. T. Ramesh, and A. M. Okamura, "Needle-tissue interaction forces for bevel-tip steerable needles," in *Biomedical Robotics and Biomechatronics, 2008. BioRob 2008. 2nd IEEE RAS & EMBS International Conference on*, 2008, pp. 224-231.

[41] S. Misra, K. B. Reed, K. T. Ramesh, and A. M. Okamura, "Observations of needle-tissue interactions," *Conf Proc IEEE Eng Med Biol Soc*, vol. 2009, pp. 262-5, 2009.

[42] A. Majewicz, S. P. Marra, M. G. van Vledder, M. Lin, M. A. Choti, D. Y. Song, *et al.*, "Behavior of tip-steerable needles in ex vivo and in vivo tissue," *IEEE Trans Biomed Eng*, vol. 59, pp. 2705-15, Oct 2012.

[43] S. F. Bensamoun, L. Robert, G. E. Leclerc, L. Debernard, and F. Charleux, "Stiffness imaging of the kidney and adjacent abdominal tissues measured simultaneously using magnetic resonance elastography," *Clinical imaging*, vol. 35, pp. 284-287, 2011.

[44] L. Zhai, J. Madden, W.-C. Foo, V. Mouraviev, T. J. Polascik, M. L. Palmeri, *et al.*, "Characterizing stiffness of human prostates using acoustic radiation force," *Ultrasonic imaging*, vol. 32, pp. 201-213, 2010.

[45] G. Gherardi, *Fine-Needle Biopsy of Superficial and Deep Masses: Interventional Approach and Interpretation Methodology by Pattern Recognition*: Springer Science & Business Media, 2010.

[46] N. V. Datla, B. Konh, M. Honarvar, T. K. Podder, A. P. Dicker, Y. Yu, *et al.*, "A model to predict deflection of bevel-tipped active needle advancing in soft tissue," *Med Eng Phys*, vol. 36, pp. 285-93, Mar 2014.

[47] Y. R. Van Veen, A. Jahya, and S. Misra, "Macroscopic and microscopic observations of needle insertion into gels," *Proceedings of the Institution of Mechanical Engineers, Part H: Journal of Engineering in Medicine*, vol. 226, pp. 441-449, 2012 2012.

[48] J. A. Engh, G. Podnar, D. Kondziolka, and C. N. Riviere, "Toward effective needle steering in brain tissue," in *Engineering in Medicine and Biology Society, 2006. EMBS'06. 28th Annual International Conference of the IEEE*, 2006, pp. 559-562.

[49] A. Majewicz, T. R. Wedlick, K. B. Reed, and A. M. Okamura, "Evaluation of robotic needle steering in ex vivo tissue," in *Robotics and Automation (ICRA), 2010 IEEE International Conference on*, 2010, pp. 2068-2073.

[50] P. J. Swaney, J. Burgner, H. B. Gilbert, and R. J. Webster III, "A flexure-based steerable needle: high curvature with reduced tissue damage," *IEEE Trans Biomed Eng*, vol. 60, pp. 906-9, Apr 2013.

[51] D. S. Minhas, J. A. Engh, M. M. Fenske, and C. N. Riviere, "Modeling of needle steering via duty-cycled spinning," in *Engineering in Medicine and Biology Society, 2007. EMBS 2007. 29th Annual International Conference of the IEEE*, 2007, pp. 2756-2759.

[52] N. A. Wood, K. Shahrour, M. C. Ost, and C. N. Riviere, "Needle steering system using duty-cycled rotation for percutaneous kidney access," in *Engineering in Medicine and Biology Society (EMBC),*

2010 Annual International Conference of the IEEE, 2010, pp. 5432-5435.

[53] R. J. Webster III, J. S. Kim, N. J. Cowan, G. S. Chirikjian, and A. M. Okamura, "Nonholonomic Modeling of Needle Steering," *The International Journal of Robotics Research*, vol. 25, pp. 509-525, May-Jun 2006.

[54] M. Mathis, D. Thompson, B. Addis, and D. F. Yankelevitz, "Steerable device for accessing a target site and methods," 2015.

[55] B. T. Sitzman and D. R. Uncles, "The effects of needle type, gauge, and tip bend on spinal needle deflection," *Anesth Analg*, vol. 82, pp. 297-301, Feb 1996.

[56] T. R. Wedlick and A. M. Okamura, "Characterization of pre-curved needles for steering in tissue," in *2009 Annual International Conference of the IEEE Engineering in Medicine and Biology Society*, 2009, pp. 1200-1203.

[57] K. B. Reed, V. Kallem, R. Alterovitz, K. Goldbergxz, A. M. Okamura, and N. J. Cowan, "Integrated planning and image-guided control for planar needle steering," in *2008 2nd IEEE RAS & EMBS International Conference on Biomedical Robotics and Biomechatronics*, 2008, pp. 819-824.

[58] Z. Chen and Y. Chen, "Analysis of multi-hinge compliant needle insertion," in *2009 IEEE International Conference on Virtual Environments, Human-Computer Interfaces and Measurements Systems*, 2009, pp. 314-318.

[59] S. Y. Ko and L. Frasson, "Closed-loop planar motion control of a steerable probe with a "programmable bevel" inspired by nature," *Robotics, IEEE Transactions on*, vol. 27, pp. 970-983, 2011.

[60] D. S. Minhas, J. A. Engh, and C. N. Riviere, "Testing of neurosurgical needle steering via duty-cycled spinning in brain tissue in vitro," in *Engineering in Medicine and Biology Society, 2009. EMBC 2009. Annual International Conference of the IEEE*, 2009, pp. 258-261.

[61] D. Glozman and M. Shoham, "Flexible needle steering for percutaneous therapies," *Comput Aided Surg*, vol. 11, pp. 194-201, Jul 2006.

[62] M. O'Leary, C. Simone, T. Washio, K. Yoshinaka, and A. M. Okamura, "Robotic needle insertion: Effects of friction and needle geometry," in *Robotics and Automation, 2003. Proceedings. ICRA'03. IEEE International Conference on*, 2003, pp. 1774-1780.

[63] A. M. Okamura, C. Simone, and M. D. O'Leary, "Force modeling for needle insertion into soft tissue," *IEEE Trans Biomed Eng*, vol. 51, pp. 1707-16, Oct 2004.

[64] N. Chentanez, R. Alterovitz, D. Ritchie, L. Cho, K. K. Hauser, K. Goldberg, *et al.*, *Interactive simulation of surgical needle insertion and steering* vol. 28: ACM, 2009.

[65] V. K. Bui, S. Park, J.-O. Park, and S. Y. Ko, "Design and evaluation setup of a novel steerable flexible needle for percutaneous therapy," in *Control, Automation and Systems (ICCAS), 2015 15th International Conference on*, 2015, pp. 1839-1842.

[66] N. J. Cowan, K. Goldberg, G. S. Chirikjian, G. Fichtinger, R. Alterovitz, K. B. Reed, *et al.*, "Robotic needle steering: Design, modeling, planning, and image guidance," in *Surgical Robotics*, ed: Springer, 2011, pp. 557-582.

[67] S. A. Thompson, "An overview of nickel–titanium alloys used in dentistry," *International endodontic journal*, vol. 33, pp. 297-310, 2000.

[68] W. Gander, G. H. Golub, and R. Strebel, "Least-squares fitting of circles and ellipses," *BIT Numerical Mathematics*, vol. 34, pp. 558-578, 1994.

[69] S. Polinder, M. Y. Homs, P. D. Siersema, and E. W. Steyerberg, "Cost study of metal stent placement vs single-dose brachytherapy in the palliative treatment of oesophageal cancer," *Br J Cancer*, vol. 90, pp. 2067-72, Jun 1 2004.

[70] T. Sprang, "Ovipositor-inspired needle insertion without a net push force," MSc, Biomechanical Engineering, Delft University of Technology, Delft, 2014.

[71] D. J. Van Gerwen, J. Dankelman, and J. J. Van den Dobbelsteen, "Needle–tissue interaction forces–A survey of experimental data," *Medical engineering & physics*, vol. 34, pp. 665-680, 2012.

[72] T. K. Podder, D. P. Clark, D. Fuller, J. Sherman, W. S. Ng, L. Liao, *et al.*, "Effects of velocity modulation during surgical needle insertion," in *27th Annual Conference of the Engineering in Medicine and Biology Society (IEEE-EMBS 2005), Shanghai, China, Sept*, 2005, pp. 1-4.

[73] J. R. Crouch, C. M. Schneider, J. Wainer, and A. M. Okamura, "A velocity-dependent model for needle insertion in soft tissue," in *Medical Image Computing and Computer-Assisted Intervention - Miccai 2005, Pt 2*. vol. 3750, J. S. Duncan and G. Gerig, Eds., ed, 2005, pp. 624-632.

[74] K. Henken, D. Van Gerwen, J. Dankelman, and J. Van Den Dobbelsteen, "Accuracy of needle position measurements using fiber Bragg gratings," *Minimally Invasive Therapy & Allied Technologies*, vol. 21, pp. 408-414, 2012.

[75] I. L. Delimont, S. P. Magleby, and L. L. Howell, "Evaluating compliant hinge geometries for origami-inspired mechanisms," *Journal of Mechanisms and Robotics*, vol. 7, p. 011009, 2015.

[76] M. Goldfarb and J. E. Speich, "A well-behaved revolute flexure joint for compliant mechanism design," *Journal of Mechanical Design*, vol. 121, pp. 424-429, 1999.

[77] T. A. Krouskop, T. M. Wheeler, F. Kallel, B. S. Garra, and T. Hall, "Elastic moduli of breast and prostate tissues under compression," *Ultrason Imaging*, vol. 20, pp. 260-74, Oct 1998.

[78] M. Czerner, L. S. Fellay, M. P. Suárez, P. M. Frontini, and L. A. Fasce, "Determination of Elastic Modulus of Gelatin Gels by Indentation Experiments," *Procedia Materials Science*, vol. 8, pp. 287-296, 2015/01/01 2015.

[79] R. Righetti, J. Ophir, S. Srinivasan, and T. A. Krouskop, "The feasibility of using elastography for imaging the Poisson's ratio in porous media," *Ultrasound in medicine & biology*, vol. 30, pp. 215-228, 2004.

[80] A. I. Farrer, H. Odéen, J. de Bever, B. Coats, D. L. Parker, A. Payne, *et al.*, "Characterization and evaluation of tissue-mimicking gelatin phantoms for use with MRgFUS," *Journal of therapeutic ultrasound*, vol. 3, p. 1, 2015.

[81] F. A. Duck, *Physical properties of tissues: a comprehensive reference book*: Academic press, 2013.

[82] A. Gefen and B. Dilmoney, "Mechanics of the normal woman's breast," *Technol Health Care*, vol. 15, pp. 259-71, 2007.

APPENDIX

A. Fabrication of the interlocking mechanism designs

This part was written after consultation with the maker of the interlocking mechanism parts: Menno Lageweg from DEMO.

Cylindrical design

Several factors of the interlocking mechanism severely limited the manufacturability. First, the small diameter of the part (d = 1.2 mm) resulted in various failed attempts to create the part. Due to the part containing seven holes (⌀0.3 mm) with a thin wall (i.e., wall thickness ~0.05 mm), and six semicircles (⌀0.3 mm) shaping the outer contour, stainless steel was used after aluminum proved to not being able to withstand the manufacturing process: the walls between the holes torn during the creation. Stainless steel exhibits a larger tensile strength and provides more resistance to the possibility of the walls tearing during manufacturing. Second, the length of the part (l = 5 mm) was an issue when drilling the holes: to prevent overheating and local deformation peck drilling was used. Peck drilling involves the machine to drill part of the hole, before temporarily retracting the drill to the surface. This way, swarf is prevented from detrimentally building up inside the hole as it is removed with the reciprocal motion. Third, in order for the wires to be aligned correctly, the holes must be aligned with respect to adjacent holes. When removing the drill from the hole completely, it was found that it is not feasible to reinsert the drill and make a hole aligned with the hole that was drilled before. In order for peck drilling to be successfully used to drill the holes into the workpiece, the drills had to be kept inside the holes, and thus only a minor retraction was allowed. Last, it was difficult to produce the symmetric contour of the interlocking mechanism; the contour has to be symmetric with respect to the holes, especially to the central hole that fixed the part to the rest of the needle.

The time from the start of the manufacturing attempts to producing the first successful part was about 80 man-hours. Several approaches were considered before one was found to be successful. One approach consisted of drilling holes in a small square block of stainless steel having a height equal to the length of the to be produced interlocking mechanism. The 13 holes were drilled, after which electrical discharge machining was used to cut out a circle (d = 1.2 mm) to produce the contour and therewith the interlocking mechanism part. The center of the central hole that was drilled into the block was used as a reference point to cut the circle into the block. As a result, the contour was not aligned with the holes (i.e., the outer wall thicknesses were not equal) and thus this approach was discarded.

Compared to the previously described approach, the successful approach involved the use of a cylinder instead of a square block of stainless steel. In the cylinder, the 13 holes were drilled (feed: 25 mm/min, speed: 20,000 rpm). Subsequently, the workpiece was milled using a computer numerical control milling machine that allowed for movements of the machine in the shape of a spiral; with every rotation of the machine, the diameter of the workpiece shrank until the desired diameter of the part was met.

Conical design

To create the conical interlocking mechanisms, the same approach as for the cylindrical design was used. One of the main differences was that the holes for the outer wires were drilled into the workpiece that was under the half-angle of the cone (i.e., 2°). Another difference was that the milling machine was now fixated, while the workpiece was rotated under an angle to form the conical outer contour.

See next page for the engineering drawings of the conical and the cylindrical interlocking mechanism.

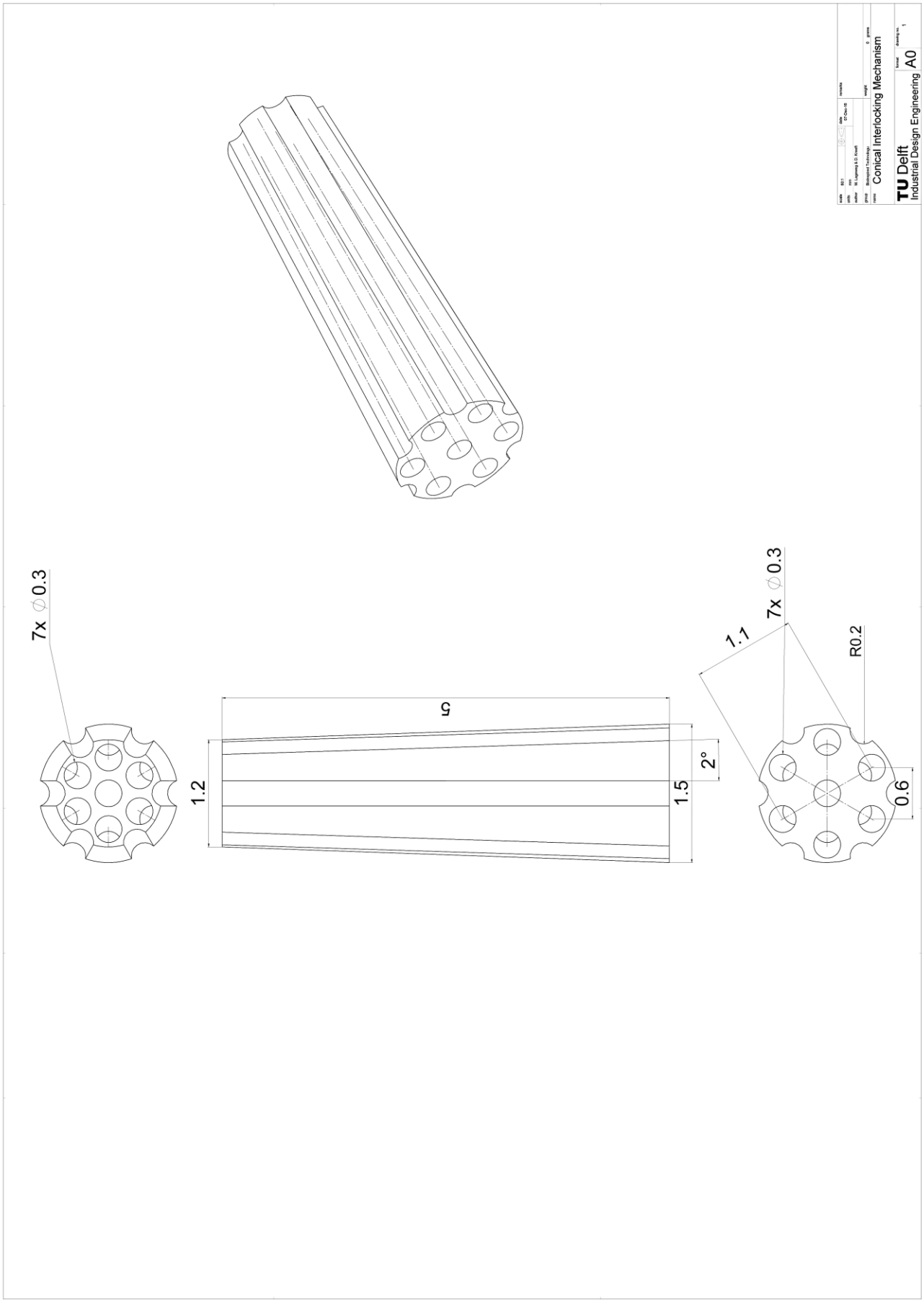
Conical Interlocking Mechanism
TU Delft
Industrial Design Engineering
A0
7x ∅ 0.3
5
1.2
1.5
2°
7x ∅ 0.3
1.1
R0.2
0.6

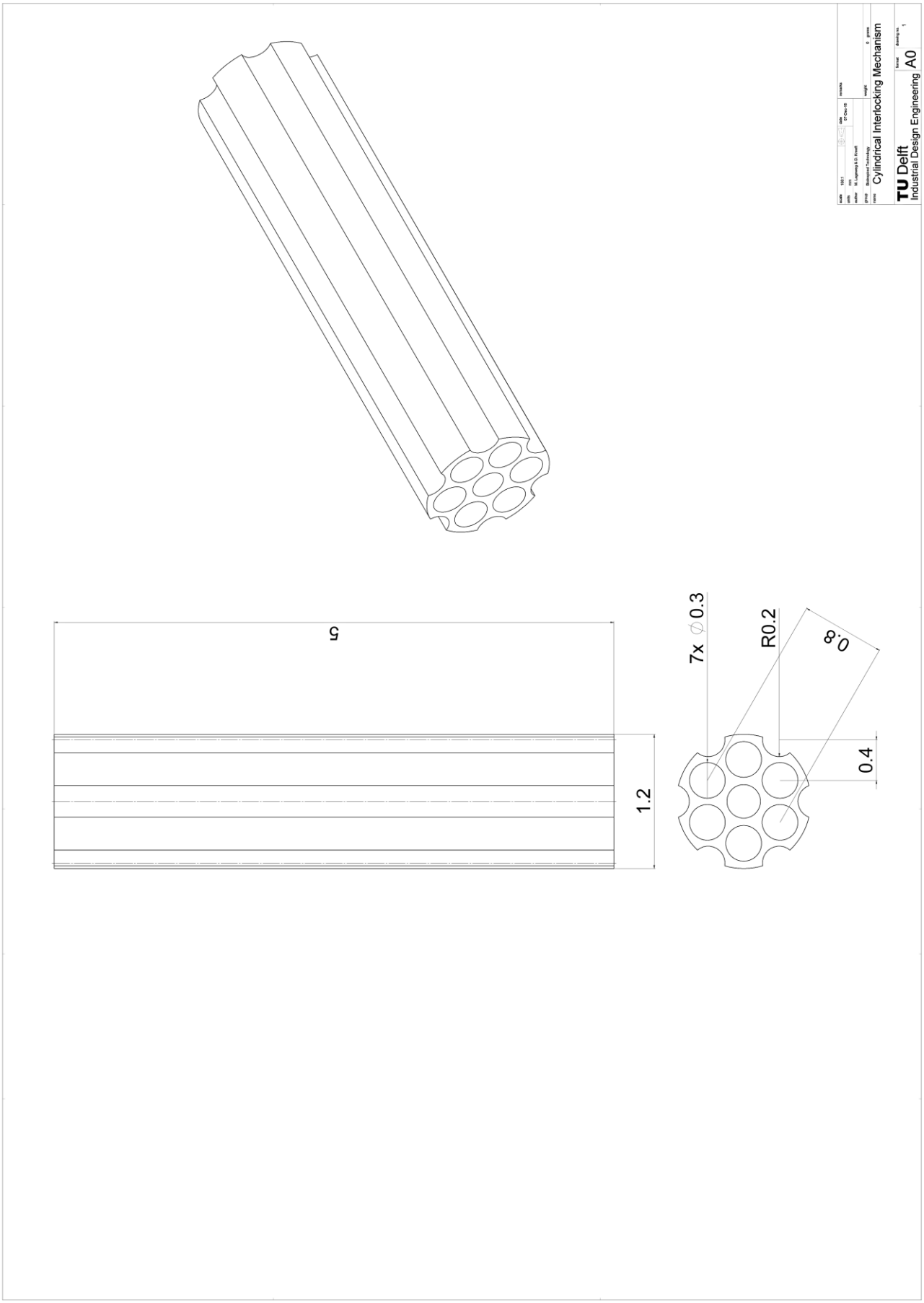
Cylindrical Interlocking Mechanism
TU Delft
Industrial Design Engineering
A0
5
1.2
7x ∅ 0.3
R0.2
0.8
0.4

B. Determining elastic modulus

Background

In order to establish the elastic modulus with a universal testing machine, the following assumptions were made: the gelatin behaves linear elastically, is incompressible (Poisson's ratio; v = 0.495), isotropic, and its temperature remains constant throughout the compression. When using these assumptions, only one parameter is required to characterize the mechanical properties: the elastic modulus [77]; that is only a function of the material and not of the geometry or boundary conditions.

The assumptions that were made are justified as follows. Assuming linear elasticity instead of hyperelasticity slightly overestimates the elastic modulus value at macroscale [78]. In addition, gelatin samples were found to have an approximately constant Poisson's ratio close to 0.5 [79]. The assumptions about isotropy is justified by testing a physically large gelatin sample. The gelatin samples are directly tested after removal from the refrigerator to ensure no influence of the heating of the samples.

Procedure

The elastic modulus of 5, 8, and 10 wt% gelatin phantoms were measured using a calibrated Zwick/Roell Z005 (Zwick GmbH & Co. KG, Ulm, Germany) universal testing machine that was equipped with a KAF-TC load cell. The machine was fitted with two acrylic (PMMA) plates measuring about 200 x 200 x 20 mm. Between these plates the gelatin samples were positioned in the center and a thin plastic film was used to minimize friction effects between the plates and the samples.

The 12 gelatin samples (i.e., four of each concentration) that were tested were made using the same procedure as described earlier, and taken out of the refrigerator shortly before positioning them one by one in between the plates. The order of the measurements was randomized using Microsoft Excel (Microsoft Office Professional Plus 2010, Version 14.0.7172.5000 (64-bit)). Next, the sample was loaded with a uniaxial compressive force of 250 N and a preload of 1%. The machine moved 8 mm down with a compressive speed equal to 16 mm/min, and the load cycle was repeated 5 times in total. Only the force and travel in the downward motion of the cycle were stored for further processing. As strain hardening effects are present inside the gelatin, a certain relaxation time has to be taken into account. Therefore, only the first load cycle of each measurement is considered.

Results

The data was initially stored in the testing software testXpert II (Zwick GmbH & Co. KG, Ulm, Germany) before being exported to MATLAB R2012b. The data was processed using a custom MATLAB file shown in Appendix H. The results are as follows. 5% gelatin: M = 4.6 kPa, SE = 0.21 kPa. 8% gelatin: M = 7.7 kPa, SE = 0.56 kPa. 10% gelatin: M = 12.2 kPa, SE = 0.45 kPa. As expected, the lower the gelatin concentration, the lower the elastic modulus and thus the less stiff the gelatin sample is.

The elastic moduli of the gelatin samples roughly correspond to brain (0.5–6 kPa [80]), muscle (in-vivo, across fibers, human, tense, 10% strain: 0.11±2% MPa [81] and 6–15 kPa [80]), and skeletal muscle, glandular (7.5–66 kPa [82]) or adipose tissue (0.5–25 kPa [82]).

C. Arduino code for moving individual wire

```
#include <GelStepper.h>

GelStepper GS;  // initialize GelStepper

// variables
//select individual wire by removing "//" and change direction of wire in line 21

//unsigned char actv = B00000001;   // wire 1
//unsigned char actv = B00000010;   // wire 2
//unsigned char actv = B00000100;   // wire 3
//unsigned char actv = B00001000;   // wire 4
//unsigned char actv = B00010000;   // wire 5
//unsigned char actv = B00100000;   // wire 6

void setup()
{
  digitalWrite(M0,0); // pin M0 for all 6 motors
  digitalWrite(M1,0); // pin M1 for all 6 motors
  digitalWrite(EN,0); // nEN for all 6 motors
  digitalWrite(SLPCFG,1); // combined nSLEEP and CONFIG pins for all 6 motors
  DIR.COMBINED.MOTORS = 0; //0: forward, 0x3F: backward.
}

void loop()
```

```
{
  STEP.COMBINED.MOTORS = actv;

  delayMicroseconds(2200);

  STEP.COMBINED.MOTORS = B00000000;

  delayMicroseconds(2200);
}
```

Which requires “GelStepper.h” to communicate with the stepper motors:

```
#ifndef GELSTEPPER_H
#define GELSTEPPER_H

// Header file for proto shield with 6 stepper motor drivers
// designed for use with the Arduino MEGA2560


// Pin locations of the configuration pins
#define M0   49
#define M1   48
#define EN   43
#define SLPCFG 42


// define the locations of all STEP and DIR pins
typedef volatile union
{
   volatile struct
   {
       volatile unsigned char MOTORS    :6;
   }COMBINED;
   volatile struct
   {
       volatile unsigned char MOT1      :1;
       volatile unsigned char MOT2      :1;
       volatile unsigned char MOT3      :1;
       volatile unsigned char MOT4      :1;
       volatile unsigned char MOT5      :1;
       volatile unsigned char MOT6      :1;
   }OF;
}INOUT;

#define STEP (*(INOUT*)&PORTA)
#define DIR (*(INOUT*)&PORTC)


// GelStepper class
class GelStepper
{
    public:
        GelStepper();
        ~GelStepper();
    protected:
    private:
};

#endif // GELSTEPPER_H
```

D. Arduino code for initial insertion

```
//This is the main sketch for initially inserting the needle.

////////////////////////////////////////////////////////////////
//////////////////////// INITIALIZATION ////////////////////////
////////////////////////////////////////////////////////////////
```

```
// SETUP.

#include <GelStepper.h> //include GelStepper library to main file
GelStepper GS;  // initialize GelStepper

#include <math.h> //inlcude maths library

#include "moveMotor.h" //include moveMotor header function to main file

// SETTINGS. This section specifies the parameter levels (such as speed, offset, bevel angle),
// actuation mode settings (such as straight/curved, single/double). The variables listed in
this section have to be set
// to the desired value (or mode) for each experiment.

float mSpeed = 1.0; //desired travel speed of selected motor in [mm/s]. Change to desired
value.
float Stroke = 4.0; //desired protrusion offset for each motor in [mm]. Change to desired
value.
//-------------------------------------------------------------------------------------------
-------------------------------------------------

// MOTORS. Binary masks for stepping individual/or combination of several motors.
unsigned char mot1 = B00000001; //mask for motor 1
unsigned char mot2 = B00000010; //mask for motor 2
unsigned char mot3 = B00000100; //mask for motor 3
unsigned char mot4 = B00001000; //mask for motor 4
unsigned char mot5 = B00010000; //mask for motor 5
unsigned char mot6 = B00100000; //mask for motor 6
unsigned char mot12 = B00000011; //mask for motor 1&2
unsigned char mot16 = B00100001; //mask for motor 1&6
unsigned char mot23 = B00000110; //mask for motor 2&3
unsigned char mot34 = B00001100; //mask for motor 3&4
unsigned char mot45 = B00011000; //mask for motor 4&5
unsigned char mot56 = B00110000; //mask for motor 5&6
unsigned char motAll = B00111111; //mask for motor 1-6
unsigned char motBev1;
unsigned char motBev2;
unsigned char motPair1;
unsigned char motPair2;
unsigned char motPair3;

// CONSTANTS (SPECIFIED AND DERIVED). All the necessary constants are specified in this
section.

boolean state = true; //'state' is toggled at the end of void loop() function to make sure it
only runs once.
String stateCheck; //String variable that let's user start the program manually.

int TDIST = 30; //total travel distance of gel-cart in [mm]

int totNumCycles = ceil(TDIST / Stroke); //number of cycles. derived from total travel distance
and desired protrusion offset. Is rounded up to the next integer.
int mDelay = round((0.2*1000000)/(mSpeed*2*20)); //time delay [us] derived from desired travel
speed. formula: LeadScrewPitch/(speed*2*stepsPerRev). stepsPerRev depends on step settings of
motor (full step mode: 20 steps for one rev.)

int ii = 1; //counter for void loop function

////////////////////////////////////////////////////////////////
//////////////////////////  START //////////////////////////////
////////////////////////////////////////////////////////////////
void setup() {

// Full step: M0,0 & M1,0
// Half step: M0,1 & M1,0
// 1/4 step:  M0,floating & M1,0
```

```
// 1/8 step:  M0,0 & M1,1
// 1/16 step: M0,1 & M1,1
// 1/32 step: M0,floating & M1,1

  digitalWrite(M0,0); // pin M0 for all 6 motors
  digitalWrite(M1,0); // pin M1 for all 6 motors
  digitalWrite(EN,0); // nEN for all 6 motors
  digitalWrite(SLPCFG,1); // combined nSLEEP and CONFIG pins for all 6 motors

  Serial.begin(9600); //opens serial port at 9600bps.

}

void loop() {

  // determine motor sequence for curved trajectory
    motBev1 = mot5;
    motBev2 = mot6;
    motPair1 = mot16;
    motPair2 = mot45;
    motPair3 = mot23;

  Serial.println("Enter 'ok' to start the initial insertion...");
  while(Serial.available()==0){     //empty while loop to wait for user
input.
  }

  stateCheck = Serial.readString(); //reads user input.

  if(ii == 1 && stateCheck != ""){     //if input is 'ok', state is toggled to 'true' and
program starts.
    state = true;
  }

  if(state == true) //this if statement makes sure void loop() does not continue running.
  {
    Serial.println("Insertion started, displaying number of completed cycles...");

        for(int numCycles = 0; numCycles <= totNumCycles-1; numCycles++) //iterate for entire
travel distance.
        {
            DIR.COMBINED.MOTORS = 0; //set direction pins forward. equal to B000000.

            moveMotor(mot12, mDelay, Stroke); //call moveMotor function for motor 1 & 2
            moveMotor(mot34, mDelay, Stroke); //call moveMotor function for motor 3 & 4
            moveMotor(mot56, mDelay, Stroke); //call moveMotor function for motor 5 & 6

            DIR.COMBINED.MOTORS = ~DIR.COMBINED.MOTORS; //reverse direction.

            moveMotor(motAll, mDelay, Stroke); //call moveMotor function for motor 1-6

            Serial.println(numCycles+1);
        }
  }
state = false; //toggle to 'false' to end void loop() function.

ii++; //counter + 1

Serial.println("Initial insertion finished");

} //void loop end
```

Which requires “MoveMotor.h”:

```
//This function is responsible for making the selected motor move. The function receives
information
// about motor, speed (i.e. delay) and protrusion offset as an input.
```

```
void moveMotor (unsigned char motorMask, int mDelay, float mOffset)
{
  int numSteps = 5*20*mOffset; // b/c 5 revolutions equal 1mm travel distance and 20
excitations are required for one rev. in full step mode.

  for(int counter = 0; counter <= numSteps-1; counter++)
  {
    STEP.COMBINED.MOTORS = motorMask;
    delayMicroseconds(mDelay);
    STEP.COMBINED.MOTORS = ~STEP.COMBINED.MOTORS & motorMask;
    delayMicroseconds(mDelay);
  }

}
```

E. Arduino code for actuating the needle

```
//This is used for actuating the needle.
//Last update: 24 July 2016

////////////////////////////////////////////////////////////////
////////////////////////// INITIALIZATION //////////////////////
////////////////////////////////////////////////////////////////

// SETUP.

#include <GelStepper.h> //include GelStepper library to main file
GelStepper GS;  // initialize GelStepper

#include <math.h> //inlcude maths library

#include "moveMotor.h" //include moveMotor header function to main file

//-------------------------------------------------------------------------------------------------
-------------------------------------------------
//--------------------------------USER INPUT-----------------------------------------------------
-------------------------------------------------
//-------------------------------------------------------------------------------------------------
-------------------------------------------------
// SETTINGS. This section specifies the parameter levels (such as stroke, offset, direction,
travelling distance),
// actuation mode settings (such as straight/curved, single/double). The variables listed in
this section have to be set
// to the desired value (or mode) for each experiment.

float mStroke = 4.0; //desired stroke for each motor in [mm].
float mOffset = 1.8; //desired offset in [mm].
String dir = "right"; //desired side to protrude, either "left" or "right".
int TDIST = 120; //theoretical travelling distance of needle in [mm]. Default is 120 mm.
float mSpeed = 1.0; //desired linear speed of selected motor in [mm/s]. Default is 1.0 mm/s.

//-------------------------------------------------------------------------------------------------
-------------------------------------------------


// MOTORS. Binary masks for stepping individual/or combination of several motors.

unsigned char mot1 = B00000001; //mask for motor 1
unsigned char mot2 = B00000010; //mask for motor 2
unsigned char mot3 = B00000100; //mask for motor 3
unsigned char mot4 = B00001000; //mask for motor 4
unsigned char mot5 = B00010000; //mask for motor 5
unsigned char mot6 = B00100000; //mask for motor 6
unsigned char mot12 = B00000011; //mask for motor 1&2
unsigned char mot13 = B00000101; //mask for motor 1&3
unsigned char mot16 = B00100001; //mask for motor 1&6
unsigned char mot23 = B00000110; //mask for motor 2&3
```

```
unsigned char mot25 = B00010010; //mask for motor 2&5
unsigned char mot34 = B00001100; //mask for motor 3&4
unsigned char mot45 = B00011000; //mask for motor 4&5
unsigned char mot56 = B00110000; //mask for motor 5&6
unsigned char mot36 = B00100100; //mask for motor 3&6
unsigned char mot35 = B00010100; //mask for motor 3&5
unsigned char mot46 = B00101000; //mask for motor 4&6
unsigned char mot123 = B00000111; //mask for motor 1&2&3
unsigned char mot456 = B00111000; //mask for motor 4&5&6
unsigned char motAll = B00111111; //mask for motor 1-6

unsigned char motBev1;
unsigned char motBev2;
unsigned char motBev3;
unsigned char motBev4;
unsigned char motPair1;
unsigned char motPair2;
unsigned char motPair3;

// CONSTANTS (SPECIFIED AND DERIVED). All the necessary constants are specified in this
section.

boolean state = true; //'state' is toggled at the end of void loop() function to make sure it
only runs once.
String stateCheck = ""; //String variable that let the actuation sequence start.
String picCheck = ""; //String to aid user input when picture needs to be taken.

int totNumCycles = ceil(TDIST / mStroke); //number of cycles. derived from total travel
distance and desired protrusion offset. Is rounded up to the next integer.
int mDelay = round((0.2*1000000)/(mSpeed*2*20)); //time delay [us] derived from desired travel
speed. formula: LeadScrewPitch/(speed*2*stepsPerRev). stepsPerRev depends on step settings of
motor (full step mode: 20 steps for one rev.)

int ii = 1; //counter for void loop function


////////////////////////////////////////////////////////////////////
//////////////////////////////  START ////////////////////////////////
////////////////////////////////////////////////////////////////////

void setup() {

// Full step: M0,0 & M1,0
// Half step: M0,1 & M1,0
// 1/4 step:  M0,floating & M1,0
// 1/8 step:  M0,0 & M1,1
// 1/16 step: M0,1 & M1,1
// 1/32 step: M0,floating & M1,1

  digitalWrite(M0,0); // pin M0 for all 6 motors
  digitalWrite(M1,0); // pin M1 for all 6 motors
  digitalWrite(EN,0); // nEN for all 6 motors
  digitalWrite(SLPCFG,1); // combined nSLEEP and CONFIG pins for all 6 motors

  Serial.begin(9600); //opens serial port at 9600bps.

}

void loop() {

  // determine motor sequence to let one side protrude and move first
  if(dir == "left"){
    motBev1 = mot1;
    motBev2 = mot6;
    motBev3 = mot5;
    motBev4 = mot4;
    motPair1 = mot16;
```

```
    motPair2 = mot45;
    motPair3 = mot23;
  }

  else if(dir == "right"){
    motBev1 = mot1;
    motBev2 = mot2;
    motBev3 = mot3;
    motBev4 = mot4;
    motPair1 = mot12;
    motPair2 = mot34;
    motPair3 = mot56;
  }

  else{
    ii = 2;
  }

  Serial.println("Enter 'ok' to start the program...");
  while(Serial.available()==0){    //empty while loop to wait for user
input.
  }

  stateCheck = Serial.readString(); //reads user input.

  if(ii == 1 && stateCheck != ""){     //if input is 'ok', state is toggled to 'true' and
program starts.
    state = true;
  }

  if(state == true) //this if statement makes sure void loop() does not continue running.
  {
    Serial.println("Program started, displaying number of completed cycles...");

    //let one chosen side protrude.
    moveMotor(motBev1, mDelay, mOffset);
    moveMotor(motBev2, mDelay, mOffset);
    moveMotor(motBev3, mDelay, mOffset);
    moveMotor(motBev4, mDelay, mOffset);

    for(int numCycles = 0; numCycles <= totNumCycles-1; numCycles++) //iterate for entire
chosen travelling distance.
        {
            DIR.COMBINED.MOTORS = 0; //set direction pins forward. equal to B000000.

            moveMotor(motPair1, mDelay, mStroke); //call moveMotor function for pair 1,
depending on side.
            moveMotor(motPair2, mDelay, mStroke); //call moveMotor function for pair 2,
depending on side.
            moveMotor(motPair3, mDelay, mStroke); //call moveMotor function for pair 3,
depending on side.

            DIR.COMBINED.MOTORS = ~DIR.COMBINED.MOTORS; //reverse direction.

            moveMotor(motAll, mDelay, mStroke); //call moveMotor function for motor 1-6 to move
backwards.

            Serial.println(numCycles+1);
        }

    Serial.println("Take photo now. Enter 'done' to continue...");
    while(Serial.available()==0){    //empty while loop to wait for user
input.
        }

    String picCheck = Serial.readString(); //read user input.
```

```
    if(picCheck != "")
        {
            Serial.println("Resetting...");
            DIR.COMBINED.MOTORS = 0x3F; //set direction pins backward. equal to B111111.
            moveMotor(motBev1, mDelay, mOffset); //reset bevel angle offset between wire 1 & 2
by moving motor 2
            moveMotor(motBev2, mDelay, mOffset); //reset bevel angle offset between wire 3 & 4
by moving motor 3
            moveMotor(motBev3, mDelay, mOffset); //reset bevel angle offset between wire 1 & 2
by moving motor 2
            moveMotor(motBev4, mDelay, mOffset); //reset bevel angle offset between wire 3 & 4
by moving motor 4
        }
  }   //closes state check if-statement


state = false; //toggle to 'false' to end void loop() function.

ii++; //counter + 1

Serial.println("End of program, please restart Serial Monitor...");

} //void loop end
```

F. MATLAB code for storing Arduino variables

```
% .m-file to read the settings from an Arduino file in the same directory,
% to extract them, and to subsequently write them to a date and time
% specific .txt-file
% D. Kreeft, 3 July 2016, updated 12 July 2016
% Input: set the lines which describe the settings (line_start, line_end)

% clear workspace, close all windows, and clear command window
clear all; close all; clc;

% set start/end line of code to be extracted
line_start = 25;     % first line with a setting
line_end = 30;       % only read until the end of the settings lines

% open arduino file with unspecified name in the same directory
filename = dir('*.ino');
fid = fopen(filename.name,'r'); % read-only

% read, extract, and close arduino file
arduino = textscan(fid,'%s',line_end,'Delimiter','\n');
fclose(fid);

% only store the important lines
S = cell2struct(arduino,'text',3);
content = S.text(line_start:line_end);

% create new file to store settings
fname = sprintf('settings_%s.txt', datestr(now, 30));

% open file for writing
fid = fopen(fname, 'wt');
formatSpec = '%s\n';

% write line-by-line
for row = 1:line_end-line_start
    fprintf(fid,formatSpec,content{row});
end
fclose(fid);
```

G. MATLAB code for image processing

```
% example .m-file to process cropped images in the same directory and
% to extract the radii of the needle from those images (originally for the
% diverging interlocking mechanism, adapted for the report)
% requires: import_image.m, fitcircle.m
% D. Kreeft, 11 October 2016

% cleaning up
close all; clear all; clc

%% initialize
% import all images
disp('Importing images') % display progress
import_image

% create groups for each condition based on number of measurement
cond01 = {images{3}, images{8}, images{13}, images{15}, images{37}, ...
    images{42}, images{54}, images{59}};
cond02 = {images{9}, images{17}, images{28}, images{32}, images{38}, ...
    images{51}, images{60}, images{62}};
cond03 = {images{20}, images{25}, images{27}, images{31}, images{33}, ...
    images{47}, images{58}, images{63}};
cond04 = {images{10}, images{24}, images{26}, images{30}, images{36}, ...
    images{40}, images{55}, images{57}};
cond05 = {images{2}, images{6}, images{11}, images{14}, images{16}, ...
    images{43}, images{50}, images{64}};
cond06 = {images{1}, images{4}, images{7}, images{35}, images{41}, ...
    images{46}, images{53}, images{56}};
cond07 = {images{18}, images{21}, images{23}, images{29}, images{39}, ...
    images{45}, images{48}, images{49}};
cond08 = {images{5}, images{12}, images{19}, images{22}, images{34}, ...
    images{44}, images{52}, images{61}};

% create cell containing all conditions and their images
conds = {cond01, cond02, cond03, cond04, cond05, cond06, cond07, cond08};

% allocate images to new cells
for i=1:length(conds)
    for j=1:length(conds{i})
        curCond = conds{i};
        CRcond{j} = curCond{j};
    end
    CRconds{i} = CRcond;
end

%% Preprocessing (making images suitable for fitting a circle)
% specify two shapes used for preprocessing
SE1 = strel('diamond',10);
SE2 = strel('disk',10);

disp('Processing images') % display progress

% run loop to process every image in every condition
for jj=1:length(CRconds)
    strproc = sprintf('Processed %d condition(s) out of %d', jj, length(CRconds));
    % load a condition
    CRcond = CRconds{jj};

    % run loop to process every image in that condition
    for m=1:length(CRcond)
        %contrast stretch
        imAdj = imadjust(CRcond{m}, stretchlim(CRcond{m}), [0 1]);
        imBW = im2bw(imAdj, 0.14); % convert to black and white
        imBWInv = imcomplement(imBW); % taking complement of image
        bwarea = bwareaopen(imBWInv,26); % remove small objects
        bwdilate = imdilate(bwarea,SE1); % dilate image
        bwulti = bwulterode(bwdilate); % ultimate erode image
```

```
        clean = filledgegaps(bwulti, 173); % fill small gaps
        imProc{m} = clean; % store processed image in variable
        scF = 24.9; % convert pix to mm
    end

    imSProc{jj} = imProc; % collect all processed images
    scFs{jj} = scF; % all scaling factors
    disp(strproc) % display progress
end

%% Processing pre-processed images
% convert binary to double
for kk=1:length(imSProc)
    imProc = imSProc{kk};
    for n=1:length(imProc)
        [a, b] = find(imProc{n});
        A{n} = a;
        B{n} = b;
        C{n} = [B{n}, -A{n}];
    end
    As{kk} = A;
    Bs{kk} = B;
    Cs{kk} = C;
end

%% Fit circle to images
% use loop to fit every image
disp('Fitting circles to images') % display progress
for qq=1:length(Cs)
    strfit = sprintf('Fitted circles to %d condition(s) out of %d', qq, ...
        length(CRconds));
    C = Cs{qq};
    scF = scFs{qq};

    for o=1:length(C)
        [z, rfit] = fitcircle(C{o}(:,:));
        xfit = z(1);
        yfit = z(2);

        ang=0:0.001:2*pi;
        xp=rfit*cos(ang);
        yp=rfit*sin(ang);

        Xfit(o) = xfit;
        XfitSc(o) = xfit/scF;
        Yfit(o) = yfit;
        YfitSc(o) = yfit/scF;
        Rfit(o) = rfit;
        RfitSc(o) = rfit/scF;
        Xp{o} = xp;
        Yp{o} = yp;
    end

    Xfits{qq} = Xfit;
    XfitsSc{qq} = XfitSc;
    Yfits{qq} = Yfit;
    YfitsSc{qq} = YfitSc;
    Rfits{qq} = Rfit;
    RfitsSc{qq} = RfitSc;
    Xps{qq} = Xp;
    Yps{qq} = Yp;
    disp(strfit) % display progress
end

%% Post-processing / Check (in [1/cm])
% curvature is set to negative if needle steers in wrong direction or is
% removed when not correctly processed
```

```
%% Display box plots (with curvature correction)
disp('Plotting box plots')
% grouping curvatures
curva = [corrCurCond1'; corrCurCond2'; (10./RfitsSc{3})'; corrCurCond4';...
    corrCurCond8'; (10./RfitsSc{7})'; (10./RfitsSc{6})'; (10./RfitsSc{5})'];

groups = [ones(size(corrCurCond1')); 2*ones(size(corrCurCond2')); ...
    3*ones(size((10./RfitsSc{3})')); 4*ones(size(corrCurCond4')); ...
    5*ones(size(corrCurCond8')); 6*ones(size((10./RfitsSc{7})')); ...
    7*ones(size((10./RfitsSc{6})')); 8*ones(size((10./RfitsSc{5})'))];

% main box plots with all conditions
figure
line([0 10],[0 0])
hold on
boxplot(curva,groups,'Labels',{'O4S4L','O6S4L','O2S6L','O6S6L','O6S6R','O2S6R', ...
    'O6S4R','O4S4R'});
ylabel('Curvature [1/cm]', 'FontSize', 14,'Interpreter','LaTex')
xlabel('Conditions (O = offset, S = stroke)', 'FontSize', 14,'Interpreter','LaTex')
title( ...
'Curved experiments - Diverging interlocking mechanism - Curvatures - All conditions', ...
    'FontSize', 18,'Interpreter','LaTex')
xlabh = get(gca,'XLabel');

% display M and SE for each condition
disp(sprintf('Condition 1: M = %0.5g, SE = %0.5g [1/cm]', ...
    mean(corrCurCond1), std(corrCurCond1)/sqrt(length(corrCurCond1))))
disp(sprintf('Condition 2: M = %0.5g, SE = %0.5g [1/cm]', ...
    mean(corrCurCond2), std(corrCurCond2)/sqrt(length(corrCurCond2))))
disp(sprintf('Condition 3: M = %0.5g, SE = %0.5g [1/cm]', ...
    mean(10./RfitsSc{3}), std(10./RfitsSc{3})/sqrt(length(10./RfitsSc{3}))))
disp(sprintf('Condition 4: M = %0.5g, SE = %0.5g [1/cm]', ...
    mean(corrCurCond4), std(corrCurCond4)/sqrt(length(corrCurCond4))))
disp(sprintf('Condition 5: M = %0.5g, SE = %0.5g [1/cm]', ...
    mean(10./RfitsSc{5}), std(10./RfitsSc{5})/sqrt(length(10./RfitsSc{5}))))
disp(sprintf('Condition 6: M = %0.5g, SE = %0.5g [1/cm]', ...
    mean(10./RfitsSc{6}), std(10./RfitsSc{6})/sqrt(length(10./RfitsSc{6}))))
disp(sprintf('Condition 7: M = %0.5g, SE = %0.5g [1/cm]', ...
    mean(10./RfitsSc{7}), std(10./RfitsSc{7})/sqrt(length(10./RfitsSc{7}))))
disp(sprintf('Condition 8: M = %0.5g, SE = %0.5g [1/cm]', ...
    mean(corrCurCond8), std(corrCurCond8)/sqrt(length(corrCurCond8))))

% display the maxmimum curvature for each condition
disp(sprintf('The maximum curvature for condition 1 is %0.5g [1/cm]', ...
    max(abs(corrCurCond1))))
disp(sprintf('The maximum curvature for condition 2 is %0.5g [1/cm]', ...
    max(abs(corrCurCond2))))
disp(sprintf('The maximum curvature for condition 3 is %0.5g [1/cm]', ...
    max(abs(10./RfitsSc{3}))))
disp(sprintf('The maximum curvature for condition 4 is %0.5g [1/cm]', ...
    max(abs(corrCurCond4))))
disp(sprintf('The maximum curvature for condition 5 is %0.5g [1/cm]', ...
    max(abs(10./RfitsSc{5}))))
disp(sprintf('The maximum curvature for condition 6 is %0.5g [1/cm]', ...
    max(abs(10./RfitsSc{6}))))
disp(sprintf('The maximum curvature for condition 7 is %0.5g [1/cm]', ...
    max(abs(10./RfitsSc{7}))))
disp(sprintf('The maximum curvature for condition 8 is %0.5g [1/cm]', ...
    max(abs(corrCurCond8))))
```

Which requires “fitcircle.m”[1] to fit a circle and “import_image.m” to import the cropped images:

```
% file to import images from the current path
% D. Kreeft
```

[1] By Richard Brown, available on MATLAB File Exchange: https://mathworks.com/matlabcentral/fileexchange/15060-fitcircle-m, Accessed 15 November 2016.

```
% preallocate memory
images = cell([1 64]);      % import image 1-64 [set based on # images]

% start importing .jpg and write to images variable
for k = 1:max(size(images))
  jpgFilename = strcat(num2str(k), '.jpg');
  images{k} = imread(jpgFilename);
end
```

H. MATLAB code for processing experiments elastic moduli of gelatin

```
% File to import and process data obtained through compression tests
% Created by D. Kreeft, 6 July 2016
% Requires: importfile.m
% Last update: 13 July 2016

% clean up
close all; clear all; clc;

%% import measurements
% initialize variables
v = 0.495;      % poisson's ratio
w = 8.00e-3;    % maximum displacement [m]
% dimensions [m]
a5 = [12.45 12.4  12.2 12.15;               % length
       9.45 10.15 9.5  10.0] * 1e-2;        % width
a8 = [12.3 12.2 12.45 12.45;                % length
       9.2 9.95  9.7  9.95] * 1e-2;         % width
a10 = [12.35 12.35 12.35 12.25;             % length
       9.8   9.55  9.4   10.25] * 1e-2;     % width
area = [a10(1,:).*a10(2,:) a5(1,:).*a5(2,:) a8(1,:).*a8(2,:)];
l0 = [2.85 2.87 3.0 3.0 2.95 2.8 2.85 2.8 2.9 2.7 3.0 2.75];
numbers = (1:20)';

% preallocate for speed
force = cell(1,60);
travel = cell(1,60);
testtime = cell(1,60);
time = cell(1,60);
stress = cell(1,60);
strain = cell(1,60);

% scan directory for files
measurementFiles = dir('*.TRA');
numfiles = length(measurementFiles);
mydata = cell(1, numfiles);

% extract data from files, calculate stress and strain
for k = 1:numfiles
    filename = sprintf(measurementFiles(k).name);
    [force{k},travel{k},testtime{k},time{k}] = importfile(filename);
    stress{k} = num2cell(cell2mat(force(k))/area(ceil(k/5)));
    strain{k} = num2cell(cell2mat(travel(k))/l0(ceil(k/5)));
end

%% plot data
% 5% samples
figure(1); cla;
hold on
for n = 21:40
% for n = [21,26,31,36]
%     plot(testtime{n},force{n},'color',rand(1,3));
    plot(cell2mat(strain{n}),cell2mat(stress{n}),'color',rand(1,3));
    coefficients(n,:) = polyfit(cell2mat(strain{n}),cell2mat(stress{n}), 1);
    modulus(n) = coefficients(n,1);
```

```
end

axis tight
xlabel('Strain')
ylabel('Stress [Pa]')
grid on
title('Plot of stress vs. strain when compressing 5% gelatin')
legend(num2str(numbers),'Location','SouthEast')

% 8% samples
figure(2); cla;
hold on
for n = 41:60
% for n = [41,46,51,56]
%     plot(testtime{n},force{n},'color',rand(1,3));
    plot(cell2mat(strain{n}),cell2mat(stress{n}),'color',rand(1,3));
    coefficients(n,:) = polyfit(cell2mat(strain{n}),cell2mat(stress{n}), 1);
    modulus(n) = coefficients(n,1);
end

axis tight
xlabel('Strain')
ylabel('Stress [Pa]')
grid on
title('Plot of stress vs. strain when compressing 8% gelatin')
legend(num2str(numbers),'Location','SouthEast')

% 10% samples
figure(3); cla;
hold on
for n = 1:20
    plot(cell2mat(strain{n}),cell2mat(stress{n}),'color',rand(1,3));
    coefficients(n,:) = polyfit(cell2mat(strain{n}),cell2mat(stress{n}), 1);
    modulus(n) = coefficients(n,1);
end

axis tight
xlabel('Strain')
ylabel('Stress [Pa]')
grid on
title('Plot of stress vs. strain when compressing 10% gelatin')
legend(num2str(numbers),'Location','SouthEast')

% Determine the elastic modulus of the specimens
elastic_modulus = struct('five',modulus(21:40),'eight',modulus(41:60),'ten',modulus(1:20));
disp('The elastic moduli [Pa] for 5% gelatin are:')
disp(sprintf('%0.4d',elastic_modulus.five(1)))
disp(sprintf('%0.4d',elastic_modulus.five(6)))
disp(sprintf('%0.4d',elastic_modulus.five(11)))
disp(sprintf('%0.4d',elastic_modulus.five(16)))

disp('The elastic moduli [Pa] for 8% gelatin are:')
disp(sprintf('%0.4d',elastic_modulus.eight(1)))
disp(sprintf('%0.4d',elastic_modulus.eight(6)))
disp(sprintf('%0.4d',elastic_modulus.eight(11)))
disp(sprintf('%0.4d',elastic_modulus.eight(16)))

disp('The elastic moduli [Pa] for 10% gelatin are:')
disp(sprintf('%0.4d',elastic_modulus.ten(1)))
disp(sprintf('%0.4d',elastic_modulus.ten(6)))
disp(sprintf('%0.4d',elastic_modulus.ten(11)))
disp(sprintf('%0.4d',elastic_modulus.ten(16)))

% calculate M and SE for each concentration
mean5 = mean(elastic_modulus.five([1,6,11,16]));
se5 = std(elastic_modulus.five([1,6,11,16]))/sqrt(4);
mean8 = mean(elastic_modulus.eight([1,6,11,16]));
```

```
se8 = std(elastic_modulus.eight([1,6,11,16]))/sqrt(4);
mean10 = mean(elastic_modulus.ten([1,6,11,16]));
se10 = std(elastic_modulus.ten([1,6,11,16]))/sqrt(4);

% display the results
disp(sprintf('The elastic moduli for 5%% gelatin: M = %0.3g, SE = %0.5g [Pa]', mean5, se5))
disp(sprintf('The elastic moduli for 8%% gelatin: M = %0.3g, SE = %0.5g [Pa]', mean8, se8))
disp(sprintf('The elastic moduli for 10%% gelatin: M = %0.3g, SE = %0.5g [Pa]', mean10, se10))
```

Which requires “importfile.m” to import the measurements of the universal testing machine:

```
function [force,travel,testtime,time] = importfile(filename)
%IMPORTFILE3 Import numeric data from a text file as column vectors.
%   [STRAIN,FORCE,TRAVEL,TESTIME,TIME] = IMPORTFILE3(FILENAME) Reads data
%   from text file FILENAME for the default selection.
%
%   [STRAIN,FORCE,TRAVEL,TESTIME,TIME] = IMPORTFILE3(FILENAME, STARTROW,
%   ENDROW) Reads data from rows STARTROW through ENDROW of text file
%   FILENAME.
%
% Example:
%   [strain,force,travel,testime,time] = importfile3('5sample11.csv',1,
%   3511);
%
%    See also TEXTSCAN.

% Auto-generated by MATLAB on 2016/07/09 14:26:37
% Adapted by D. Kreeft on 2016/07/09


%% Initialize variables.
delimiter = ';';
startRow = 1;
endRow = inf;

%% Read columns of data as strings:
% For more information, see the TEXTSCAN documentation.
formatSpec = '%*21s%21s%21s%21s%21s%21s%21s%21s%[^\n\r]';

%% Open the file.
fileID = fopen(filename,'r');

%% Read columns of data according to format string.
% This call is based on the structure of the file used to generate this
% code. If an error occurs for a different file, try regenerating the code
% from the Import Tool.
dataArray = textscan(fileID, formatSpec, endRow(1)-startRow(1)+1, 'Delimiter', '',
'WhiteSpace', '', 'HeaderLines', startRow(1)-1, 'ReturnOnError', false);
for block=2:length(startRow)
    frewind(fileID);
    dataArrayBlock = textscan(fileID, formatSpec, endRow(block)-startRow(block)+1, 'Delimiter',
'', 'WhiteSpace', '', 'HeaderLines', startRow(block)-1, 'ReturnOnError', false);
    for col=1:length(dataArray)
        dataArray{col} = [dataArray{col};dataArrayBlock{col}];
    end
end

%% Close the text file.
fclose(fileID);

%% Convert the contents of columns containing numeric strings to numbers.
% Replace non-numeric strings with NaN.
raw = repmat({''},length(dataArray{1}),length(dataArray));
for col=1:length(dataArray)-1
    raw(1:length(dataArray{col}),col) = dataArray{col};
end
```

```
numericData = NaN(size(dataArray{1},1),size(dataArray,2));

for col=[1,2,3,4,5]
    % Converts strings in the input cell array to numbers. Replaced non-numeric
    % strings with NaN.
    rawData = dataArray{col};
    for row=1:size(rawData, 1);
        % Create a regular expression to detect and remove non-numeric prefixes and
        % suffixes.
        regexstr = '(?<prefix>.*?)(?<numbers>([-]*(\d+[\,]*)+[\.]{0,1}\d*[eEdD]{0,1}[-
+]*\d*[i]{0,1})|([-]*(\d+[\,]*)*[\.]{1,1}\d+[eEdD]{0,1}[-+]*\d*[i]{0,1}))(?<suffix>.*)';
        try
            result = regexp(rawData{row}, regexstr, 'names');
            numbers = result.numbers;

            % Detected commas in non-thousand locations.
            invalidThousandsSeparator = false;
            if any(numbers==',');
                thousandsRegExp = '^\d+?(\,\d{3})*\.{0,1}\d*$';
                if isempty(regexp(thousandsRegExp, ',', 'once'));
                    numbers = NaN;
                    invalidThousandsSeparator = true;
                end
            end
            % Convert numeric strings to numbers.
            if ~invalidThousandsSeparator;
                numbers = textscan(strrep(numbers, ',', ''), '%f');
                numericData(row, col) = numbers{1};
                raw{row, col} = numbers{1};
            end
        catch me
        end
    end
end


%% Exclude rows with non-numeric cells
% J = ~all(cellfun(@(x) (isnumeric(x) || islogical(x)) && ~isnan(x),raw),2); % Find rows with
non-numeric cells
raw(1,:) = [];

%% Allocate imported array to column variable names
% strain = cell2mat(raw(:, 1));
force = cell2mat(raw(:, 2));
travel = cell2mat(raw(:, 3));
testtime = str2num(cell2mat(raw(:, 6)));
time = str2num(cell2mat(raw(:, 7)));
```